LASER
& PHOTONICS
REVIEWS

Laser Photonics Rev. **9,** No. 6, 604–627 (2015) / **DOI** 10.1002/lpor.201500045

REVIEW ARTICLE

Abstract This paper provides an up-to-date overview on the use of microstructured optical fibers (MOFs) in chemical sensing during the last ten years, more specifically, applications in liquid media including the use of solid-core photonic crystal fibers, hollow-core PCFs and other MOFs and related microstructures. To this aim, a classification of different types of fiber-based chemical sensors is first made, followed by a description of the most important MOFs and their operation principles in chemical sensing. Then, studies on the use of MOFs in fluorescence, Raman and SERS detection among other detection principles are discussed. Finally, literature including the implementation of these microstructures in home-made and commercial analytical equipment is summarized. This review intends not only to give a current perspective on the use of MOFs and microstructures in chemical sensing, but also to make an approach between the fields of optical fiber and analytical chemistry, in order to understand the basic principles of operation in this promising frontier of knowledge.

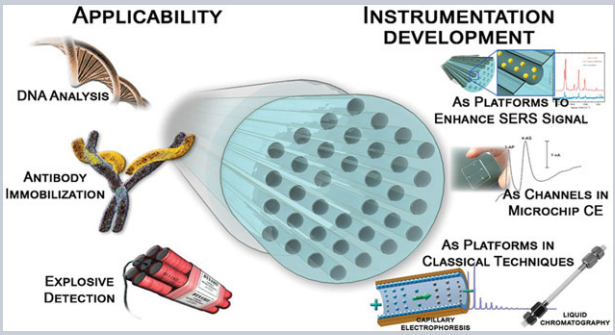

Chemical and biochemical sensing applications of microstructured optical fiber-based systems

Matías Calcerrada[1,*], Carmen García-Ruiz[1], and Miguel González-Herráez[2]

Abbreviations

AU (absorbance units); CE (capillary electrophoresis); COC (cyclic olefin copolymer); DC-PCF (defected-core photonic crystal fiber); DNA (deoxyribonucleic acid); DNB (Dinitrobenzene); FCS (fluorescence correlation spectroscopy); FPR (Fabry–Perot resonator); HC-PCF (hollow-core photonic crystal fiber); HPLC (high-performance liquid chromatography); HSW (hollow silica waveguide); ID (internal diameter); LC-PCF (liquid-core photonic crystal fiber); LOD (limit of detection); MMF (multimode fiber); MOF (microstructured optical fiber); MSC (microstructured capillary); OD (outer diameter); PCF (photonic crystal fiber); PMMA (poly(methyl methacrylate); RI (refractive index); RIU (refractive index units); SC-PCF (solid-core photonic crystal fiber); SEM (scanning electron microscope); SERS (surface-enhanced Raman spectroscopy); SMF (single-mode fiber); SP-PCF (strong penetration photonic crystal fiber); SPR (surface plasmon resonance); TIR (total internal reflection); USP (United States Pharmacopea unit); UV (ultraviolet); UV-Vis (ultraviolet-visible); WGM (whispering-mode resonance); α-CRP (C-reactive protein);

1. The role of optical fibers in chemical sensing

An optical fiber is a flexible, transparent thread made of high-quality silica, soft glass or polymer. It is usually used as a medium for telecommunication because of its large transmission bandwidth, low cost and flexibility. It is especially advantageous for long-distance communications, as light propagates through the fiber with little attenuation compared to electrical cables. Optical fibers have been developed since the 1970s [1–4]. In these structures, light can propagate along the fiber in a single-mode (single-mode fibers, SMF) or multiple modes (multimode fibers, MMF), depending on the core diameter and the refractive-index (RI) contrast between core and cladding. Figure 1A left shows a scheme of this type of fiber.

In the 1990s and the beginning of this century, a different type of fiber structures was conceived, called microstructured optical fibers (MOF) [5–8], in which air holes were developed along the fiber structure. Figure 1A right shows an example of MOF. These structures can lead to many different types of interesting propagation effects and a wide variety of the propagation parameters. Due to its ability to confine light in hollow cores or with confinement characteristics not possible in conventional optical fibers, MOFs are applied in fiber lasers, nonlinear devices, high-power transmission, supercontinuum light sources, high-power rod amplifiers, or highly sensitive sensors [9].

Considering their high versatility, fibers play an important role in sensing applications. SMFs and MMFs have been employed for physical and chemical sensors for the last 30 years [10–14]. For instance, Polynkin et al. designed an optical fiber sensing device to measure the RI of liquids using a tapered fiber [15]. El-Sherif et al., used optical fibers

[1] Department of Analytical Chemistry, Physical-Chemistry and Chemical Engineering, Multipurpose Building of Chemistry, University of Alcalá, Madrid 28871, Spain
[2] Department of Electronics, Polytechnic School, University of Alcalá, Madrid 28871, Spain
*Corresponding author: e-mail: matias.calcerrada@uah.es

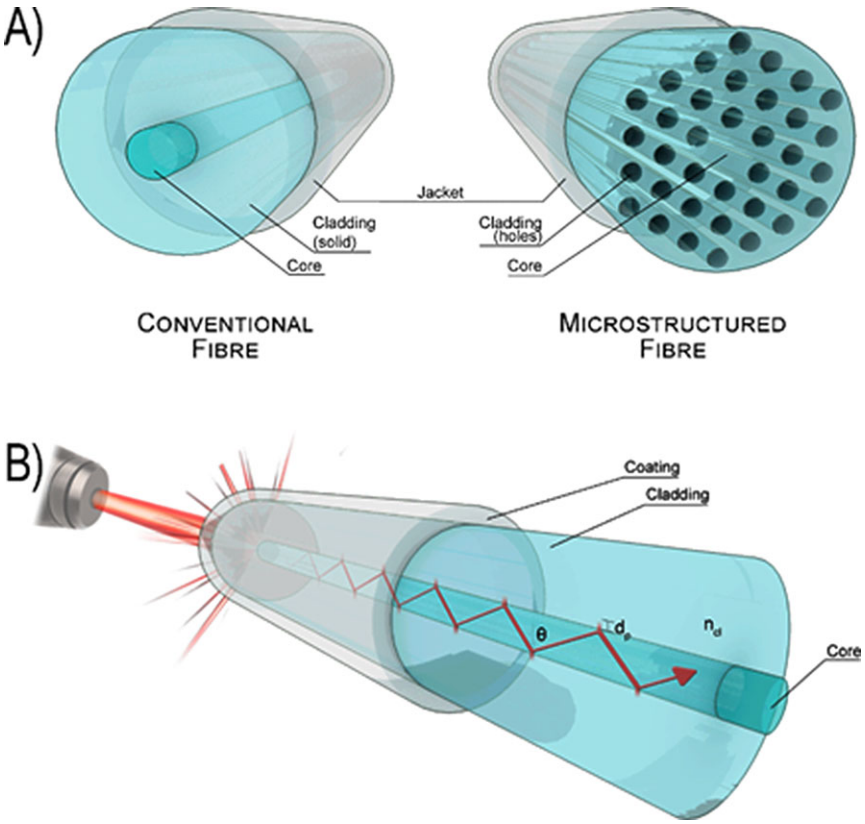

Figure 1 (A) Scheme of a conventional fiber (left) and a MOF (right) and their principal components; (B) scheme showing the light guiding through the core of a conventional fiber by TIR.

for the analysis of toxic and biological vapors for military purposes, by recording changes in any modification produced in the optical properties of the fibers [16]. In other cases, fiber is used to connect a nonfiber optic sensor to a measurement system. They are also useful in sensing strain, temperature, pressure, flow and other parameters by modifying their physical properties [17]. For example, Zheng et al. used interior nanofilm-coated fibers long-period gratings as humidity sensors, showing high sensitivity [18]. Nowadays, optical fibers in chemical-sensing systems are showing unique applications [19, 20]. In fact, reviews concerning the use of fiber optics in different parts of analytical systems and with a wide range of purposes have been recently collected in the literature [21–23].

This review focuses on MOFs and their versatility to develop novel (bio)chemical-sensing systems [24]. These structures were first used for sensing purposes in 1999, when Monro et al. proposed for the first time the use of the evanescent field within a solid-core photonic crystal fiber (SC-PCF) for making devices sensitive to the material within the holes. As shown in Fig. 1B, in these structures light is guided by TIR, thus the evanescent field allows interaction between the light fraction in this zone and the analytes inside the holes surrounding the fiber core [25, 26]. Later, other MOFs called suspended-core PCFs were fabricated, showing a larger overlap between light and analyte [27, 28]. In parallel, Cregan et al. proposed new structures in which light was guided through a hollow core. These structures, contrary to the previous ones, guide light by the bandgap effect, a totally different principle that allowed trapping the light in certain wavelength bands in a hollow core [29, 30]. These structures, called hollow-core PCF (HC-PCF), were soon proposed as ideal platforms for sensing purposes. Benabid et al. demonstrated stimulated Raman scattering in a hydrogen-filled HC-PCF [31], and other authors such as Fini also demonstrated the efficiency of HC-PCFs in chemical sensing, with analyte–light overlaps over 90% [32]. Their applicability for gas sensing [33] or Raman spectroscopy [34] was also demonstrated. Since then, great efforts have been made with the aim of developing novel and efficient fiber-based chemical-sensing devices. This review discusses the most relevant articles on analytical and bioanalytical sensing in liquid media through MOFs as a promising platform. In addition, related structures not designed for waveguiding are being employed for chemical and biochemical sensing applications, thus a general overview of the most recent studies is also useful to know the state-of-the-art of this promising frontier of knowledge. This manuscript not only reviews recent papers on this topic, but it also describes the fundamentals of these structures to use them in analytical and bioanalytical approaches. Thus, the first part of the manuscript describes the different fiber-based chemical sensors and fundamentals of the different designs. Afterwards, the different types and manufacturing processes involving MOFs are shown, to finally describe the most relevant works during previous years regarding the use of MOFs and related structures for chemical and biochemical analysis in liquid media. In addition, works that have employed MOFs and microstructures as sensing platform in classical analytical

instrumentation and their implementation in conventional systems are discussed, to finally give a general overview of the state-of-the-art in this convergent field between photonics and analytical chemistry.

2. Classification of sensors

Fibers and related microstructures are great candidates for chemical sensing due to some of their properties: they are mechanically flexible, versatile and small, thus minimal sample volumes are needed for chemical detection. In addition, small fragments are efficient enough to detect and quantify compounds, making them ideal for lab-on-a-chip and portable equipment.

Depending on the function of the structure, sensors based on fibers and related microstructures can be classified into extrinsic (here fibers are used only to guide light, thus there is no sensing region in the fiber), intrinsic (where fibers guide light and, at the same time, there is a sensing region in some part of the structure), and finally other microstructured-based sensors that employ, for example, multihole capillaries and other microstructures (which are used to enhance the sensitivity and no light guidance is required or desired).

Therefore, before describing the applications of MOFs and related microstructures in chemical-sensing systems, the different types of sensors and their basic sensing principles are described in this section. In addition, some sensing strategies have been proposed over previous years to enhance the sensitivity of these systems, thus the last subheading collects some representative examples of these strategies to achieve enhanced sensing systems.

2.1. Extrinsic sensors

Extrinsic sensors usually employ SMF or MMF (Fig. 1A left) to solely transport light from the source to the recipient where the analyte is contained. Here, the fiber is used due to its exceptional light-guiding properties, but these systems do not benefit from the fiber structure for chemical-sensing purposes. Many analytical instruments employ fibers to transport light from the laser source to the sensing region and/or from the sensing region to the detector. For example, laser-induced fluorescence or UV-Vis detectors are used in conventional analytical chemistry instrumentation and consist of lasers or lamps where optical fibers transport and collect the light. As this review focuses on sensing systems that employ microstructures, extrinsic sensors are not in the scope and will not be included.

2.2. Intrinsic sensors

Regarding intrinsic sensors, light–analyte interaction occurs inside or on the fiber, but depending on the structure, the sensing principle will be different. Therefore, conventional-fiber sensors and MOF sensors can be differentiated. Also, note that interaction between light and analyte can be made in the extremes of these structures, thus fiber-tip sensors can also be considered here.

2.2.1. Conventional-fiber intrinsic sensors

In these systems, conventional fibers are employed to carry out the interaction between light and analyte. As depicted in Fig. 1A, an optical fiber consists of a cylindrical tube, classically made of silica, though other materials like polymers or soft glass can be used as well, and with three differentiable parts: the core, the cladding, and the coating. The core is the central region, the cladding is the surrounding part, and the coating is the protective jacket, usually made of polymer, which provides tighter bend radii of optical fibers. Classical optical fibers (Fig. 1A, left) have both the core and the cladding made of silica. The silica core is usually doped with Ge to increase the RI of this medium. This difference in RI ($RI_{co} > RI_{cl}$) produces a phenomena known as total internal reflection (TIR). In general terms, with TIR, the light is guided throughout the core, avoiding losses along the optical fiber (Fig. 1(B)). This property makes optical fibers ideal for telecommunications, as those structures can transmit light signals along kilometers with low attenuation. However, a minimal part of this light is not guided through the center, and propagates in the surroundings of the core, a phenomenon known as the evanescent field, which is depicted in Fig. 1B [35, 36].

On the basis of this principle, both for SMF and MMF (Fig. 1A, left), the core and the cladding have to be removed in order to create a sensing region where the interaction between the light fraction of the evanescent field and the analyte takes place. Figure 2A shows one possible scheme where the cladding is removed to measure an analyte, in this case, nitrite concentration in water samples [37]. However, fibers were made to confine light and due to this reason, the penetration depth is so low (typically less than 1% of the light comes out of the core), that the interaction between the light and the analyte is too weak [38]. Due to this reason, studies regarding the influence of the cladding in optical-fiber sensor performance have been reported in the literature, as penetration depth will depend on the fiber structure [39]. Also, the fiber without the cladding becomes very fragile and nonpractical for routine analyses. Other perturbations can be made on the surface of the fiber, such as heating the fiber to form diameter variations with the aim of obtaining defects that cause light-propagation losses and hence more interaction with the analyte allocated in the surrounding part of the core. In addition, U-shaped optical fibers are employed to enhance sensitivity. Figure 2B depicts one scheme used to measure the oxygen concentration in air, where a U-Shaped geometry was selected to enhance the sensitivity of the system [40]. Other examples include the use of U-shaped optical fiber systems for vapor-phase detection of explosives like 2,4,6-trinitrotoluene and cyclotrimethylenetrinitramine [41], or the detection and quantification of melamine, frequently added in products (e.g.

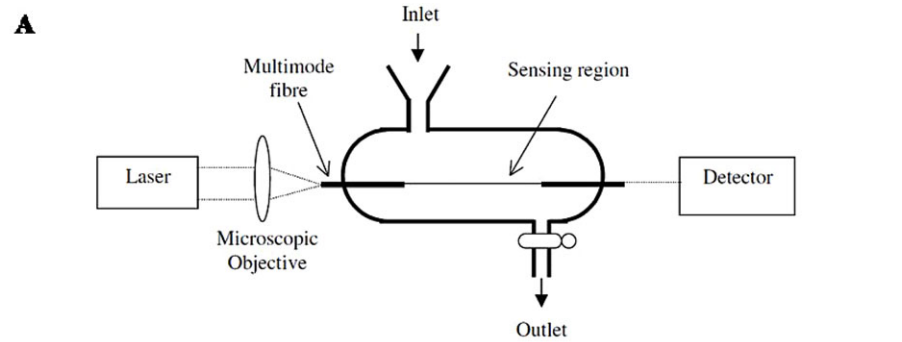

Figure 2 (A) One experimental setup where the cladding of a MMF is removed to measure the nitrite concentration in the water surrounding the core. Figure taken from [37] with permission of IOP Science. In (B) another more complex setup to measure the oxygen concentration where a U-shaped geometry is selected to enhance the sensitivity. Figure taken from [40] with permission of Elsevier.

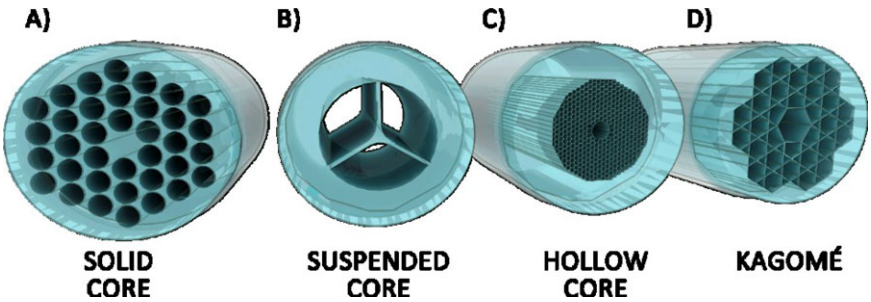

Figure 3 Schemes showing some typical structures of MOFs used in chemical sensing: (A) SC-PCF; (B) suspended-core MOF; (C) HC-PCF; and (D) Kagomé HC-MOF.

milk) to increase their protein values, but with prejudicial side effects for human health [42]. On the other hand, the use of fiber loop resonators have been recently used in SMF to enhance the sensitivity in the evanescent-field area of the systems [43–46].

2.2.2. MOF intrinsic sensors

When using MOFs different sensing strategies can be used depending on the geometry of the internal structure, i.e. the type of MOF, and also the RI of the fluids and fiber materials. There are some typical designs widely employed for sensing. Figure 3 shows different types of MOFs such as SC-PCF, a specific type of SC-MOF called a suspended-core MOF, HC-PCFs and a kagomé HC-MOF. PCFs possess a periodic arrangement of holes in the cladding, as can be seen in Fig. 3A, however, this term is often employed when propagation of light occurs due to a photonic defect or bandgap defect.

Depending on the structure employed, two different intrinsic sensors can be described:

- SC-MOFs comprising SC-PCFs and suspended-core MOFs intrinsic sensors. These sensors employ fibers that have a solid core, whereas the fluids with the analyte of interest are injected into the cladding holes. Therefore, the fraction of light on the surroundings of the core will overlap with the surrounding holes of the fiber through the evanescent-field effect.
- HC-MOF comprising HC-PCFs and Kagomé HC-MOFs intrinsic sensors. Contrary to the previous case, this sensor employs a fiber that possesses a hollow core. Therefore, under nonselective filling of the structure, interaction between light and analytic will occur under the photonic bandgap effect, where the interaction between light and analyte is much higher than for SC-MOFs.

Note that, however, different modifications and strategies can be performed on these fibers in order to increase the sensitivity of the systems or the sensing principle. For example, a commercially available solid-core PCF (SC-PCF, Crystal Fibre A/S, ESM-12-01) of 10 cm length was employed to create a novel sensor architecture with a sensitivity of 38 000 nm per refractive index unit (RIU) and detection limits of 4.6×10^{-7} RIU. This novel architecture consisted of blocking all the fiber holes but one with ultraviolet (UV) curable polymer, and using it as fluid carrier with the analyte of interest (employing only a volume of 800 pL). To achieve a high sensitivity in this structure,

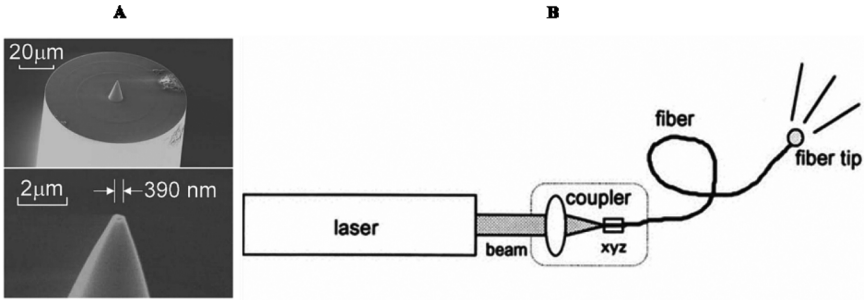

Figure 4 Example of fiber-tip-based chemical sensors. (A) SEM images of a tapered fiber for an interferometer system. Figure taken from [51] with permission of OpticsInfoBase. (B) Ball-shaped fiber tip for a medical laser system. Figure taken from [50] with permission of Springer.

fluorinated polymer PCFs were proposed as an alternative material with RI lower than the analyte solution [47]. More recently, a step-index fiber with a hollow microchannel was fabricated for the same purpose. In this case, the fiber was manufactured following the stack-and-draw technique and calculating parameters to collapse all the holes except a hollow microchannel parallel to the core. A 30-cm length of the fiber was filled with fluids of different RI and dynamic studies were carried out to demonstrate that the system was valid for areas such as nonaqueous optofluidics and RI calibration [48]. The most important strategies will be described in Section 3.

2.2.3. Fiber-tip-based sensors

The light that passes through the core of a fiber can be manipulated by using external objects or systems located on the fiber end, with the aim of increasing sensitivity or reliability of the chemical sensor. Fiber-tip chemical sensors are based on this principle, but instead of using external systems, modifications on the fiber end are made, allowing more compact, more durable, and simpler systems than those that employ external objects [49, 50]. Different fiber-tip-based sensors have been proposed, from which tapered fiber tips and others such as ball-shaped fiber tips and side-firing tips are used for chemical sensing.

Tapered fibers are constructed by increasing or decreasing the diameter of the fiber at the beginning or the end. Figure 4A shows the scanning electron microscopy (SEM) image of a tapered fiber [51]. On decreasing the fiber diameter we obtain a down tapered fiber, whereas on increasing the diameter, we have an up tapered fiber. A down taper tip spreads the light, while, on the contrary, an up taper concentrates the light in one point. With this approach, improvements in sensitivity are achieved. For example, Ran et al. employed a 157-nm laser micromachining to fabricate a cavity at the end of a SMF. This configuration allowed measurement of the external RI, producing temperature-independent measurements for fluids with RI larger than that from the air, and resolutions of approximately 4×10^{-5} RIU [52].

Coating the fiber end is another possibility to enhance the analytical sensitivity of the fiber-tip sensor [53]. In fact, some research is uniquely devoted to new methodologies for the successful deposition of nanostructures (nanoparticles, gold crescents, or nanowires) on the fiber extremes [54]. Thanks to these coatings, Raman spectroscopy performance in SMFs has been enhanced, as we will describe later in Section 3. For instance, Zheng et al. proposed the scheme depicted in Fig. 5. Here, the tip of the fiber was modified by depositing a layer of Ag nanoparticles [55]. Andrade et al. also developed a SERS sensor with a SMF with Ag nanoparticles at the fiber tip, detecting Rhodamine 6G in concentrations of 200 nM [56]. More recently, Andrade et al. also developed circular and bow tie Au nanohole arrays, which used to coat a SMF to enhance Raman signal [57]. Not only metallic coatings, but also functionalized ones have been proposed for sensing purposes. To give a representative example, Goicoechea et al. employed the layer-by-layer electrostatic self-assembly technique to fabricate an optical fiber pH sensor based on the colorimetric pH indicator neutral red. This approach, contrary to the previous works without the neutral red/(poly)acrylic acid multilayer, demonstrated higher responses times and dynamic pH ranges between 3 and 9 [58].

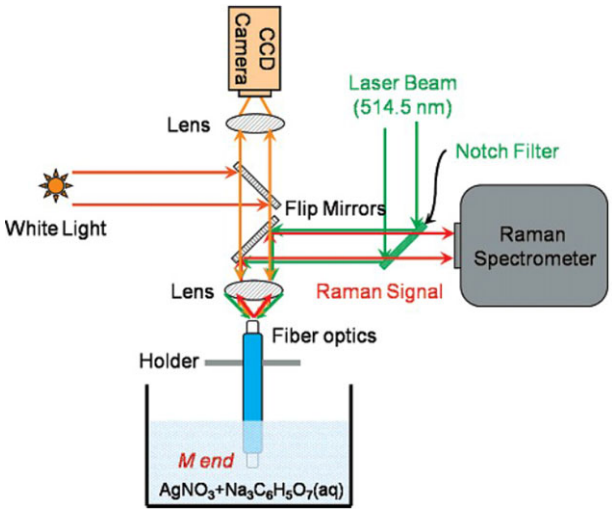

Figure 5 Scheme of a Raman spectrometer where interaction between light and the analyte takes place in the fiber tip. Figure taken from [55] with permission of ACS Publications.

In addition, standard optical fibers have proven to be useful sensors to study liquid droplets on the fiber end [59], especially for monitoring the dynamics of the evaporation process of liquid droplets of pL volumes. Preter et al. developed a simple system to undergo study of droplets of

different solvents. This simple sensor was used to measure the rate of evaporation of pL droplets, and results were in good agreement compared to direct visual examination. This sensor was also adequate to study the composition of binary systems (water/ethanol) with 2% accuracy [60].

Ball-shaped fiber tips are fibers whose end terminates at a certain curvature, or a hemispherical object is attached at the end. These fiber tips act as focusing lenses, as light beams are focused in one point near the tip. Alternatively, a fiber tip can be sculpted to a ball shape to adjust beam divergence and spot size and vary the depth of focus of a probing light source. Figure 4B shows a representative example of a ball-shaped fiber tip used for a medical application [50]. Others, like side-firing tips redirect the light over a range of angles away from the fiber axis. These sensors are often employed in therapeutic applications such as photodynamic therapy. Although they have also been employed as optical sensors for measuring the radiance distribution in turbid media [61, 62].

2.3. Other microstructured-based sensors

Finally, other types of sensing systems employ microstructures similar to MOFs that are used to enhance the sensing properties of the configurations. These systems can employ microstructures such as multihole capillaries or microstructured capillaries [63], and are usually employed in microchips or conventional analytical instrumentation to enhance the analytical performance (such as sensitivity) of the systems. Contrary to the previous systems, light is not usually guided, thus the structures are employed to enhance the performance of the systems solely, and sensing principles such as the evanescent field or bandgap effect are not present. Detailed applications of this type of sensor will be described in Sections 5.3 and 5.4.

3. Sensing mechanisms and typical strategies for sensitivity enhancement in fiber-based sensors

As described in the former configurations, sensors can be grouped regarding their sensing area (i.e. where the interaction takes place). Independently of the sensing region, different sensing mechanisms can be considered to achieve the detection of the analytes or substances of interest. In this review, the most employed optical mechanisms will be briefly described before discussing the specific applications in Section 5.

It is well known that absorbance changes can be detected when light interacts with analytes. This sensing mechanism is typical in fiber-based chemical sensors and in conventional analytical instrumentation. Although different wavelengths can be selected, UV-Vis absorption is one of the most employed light-based methods for chemical identification of analytes due to its universal nature, i.e. many analytes can be detected through their absorption changes in this region. For example, Cao and Duan employed a conventional fiber to carry out the detection of oxygen deficiency in air through changes in the absorbance, obtaining a logarithmic linear response for concentrations in the range 0.6–20.9% of oxygen [40].

Fluorescence is usually complementary to absorption spectroscopy, and it uses a beam of monochromatic light that excites the electrons in the molecules of the compounds and causes them to emit fluorescence, which is registered in the system. In contrast to absorption spectroscopy, this mechanism is much more selective but only valid when molecules present fluorescence properties, otherwise derivatization processes are required. For instance, Chu et al. were able to detect the explosive 1,4-dinitrobenzene (DN(B) in acetone, loaded in a MOF, by measuring the fluorescence decay based on the fluorescence quenching of conjugated polymers attached to the fiber surface [64].

Raman spectroscopy is another typical optical sensing mechanism that also employs a monochromatic light from a laser to observe vibrational, rotational, and other low-frequency modes in a system. This sensing mode can provide a fingerprint for each chemical specie, being therefore highly selective. Raman spectroscopy is gaining popularity over previous years in conventional analytical instrumentation and also in fiber-based chemical. However, the sensitivity of this mechanism is usually lower than the others due to the weak response of Raman signals. To enhance the signal intensity, surface-enhanced Raman spectroscopy (SERS) can be used [65–73]. The increase in sensitivity occurs because of an enhancement in the electric field provided on the surface where localized surface plasmons are excited. The use of metallic nanoparticles is extended in some chemical and biochemical applications to enhance SERS signals in different fiber-based systems.6

Finally, other sensing mechanisms consist of detecting the changes in RI. Despite being an established and well-known mechanism in the fiber-sensing field [39], this is not typical in conventional analytical instrumentation. It consists of determining the changes in RI due to the presence of analytes that are in solution or adhered to the surface of the fiber in the sensing region. Despite possessing high sensitivity, many strategies can be performed to enhance the sensitivity of these systems. Here, some representative and typical examples will be described. An interesting option for chemical sensing is the use of metallic nanoparticles. Surface plasmon resonance (SPR) based sensors have been widely used over previous years for obtaining an enhanced response to RI changes. Surface plasmons can be considered as a charge-density oscillation that may exist at the interface of two media with dielectric constants of opposite signs, being one of the media usually a metal (such as Au or Ag) [74]. In the case of SPR sensors, the metal is exposed to the analyte. The increase in sensitivity is achieved when the frequency of the incident light matches the frequency of the surface electrons of the nanoparticles. In this situation, the incident wavelength is strongly absorbed, creating a transmission dip in the sensor response. This resonant wavelength turns out to be highly sensitive to changes in the external RI, and this property makes these systems ideal for chemical sensing applications. Despite being one of the

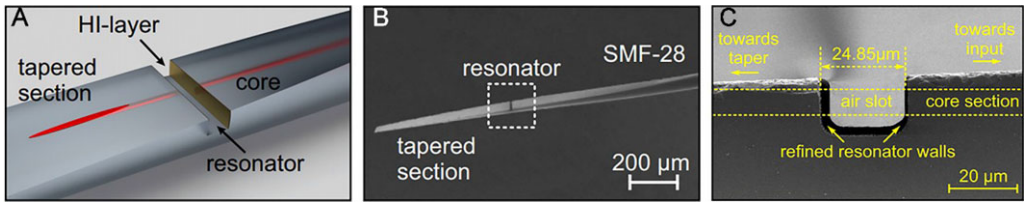

Figure 6 Example of a fiber-integrated Fabry–Perot microresonator for precise RI sensing. (A) Scheme of the in-fiber microresonator; (B) SEM image of the microresonator created in a SMF-28; (C) SEM image of the focused ion beam-milled and refined fiber-based micro-cavity. Figures taken from [96] with permission of The Optical Society.

most sensitive to RI changes, they work on specific wavelengths compared to other types of sensors [75]. To give representative examples, SPR sensors based on metallic structures such as nanoring arrays, plasmonic nanoparticles, nanoparticle pairs or nanowires have been reported in the literature [76–79]. Regarding the use of this principle in systems with optical fibers, conventional SMFs [80–83] and MMFs [84] have been widely employed. For example, Lin et al. used this principle in a SMF, depositing Au nanodot arrays with electron beam lithography. With this approach, the streptavidin concentration was determined even for minimal concentrations of 0.006 nM [85]. Recently, Sciacca and Monro developed a dip biosensor by depositing metallic nanoparticles in a SMF. An inverse relationship between the sensitivity of the system and the number of particles deposited onto the surface was demonstrated [86]. Also, setups previously commented on like U-shaped fiber sensors [87], fiber-tip-based sensors [88] or others such as D-shaped fiber sensors [89] have employed this principle to enhance sensitivity. Nevertheless, SPR sensors with MOFs and other microstructures have been less employed. For example, Wang et al. designed a first prototype of a polymeric side-hole MOF as SPR sensor [90].

Nonlinear MOFs use a sensing principle in which the dielectric polarization responds nonlinearly to the electric field of the light [7]. By using this property, nonlinear MOFs can also be used for sensing of chemicals or biomolecules. For example, the inherent nonlinear modulational instability of a long pulse in MOFs generates a Stokes and an anti-Stokes wave, whose wavelength shifts vary when a fluid is infiltrated into the holes of the MOF, being therefore valid candidates for RI measurement and chemical and biochemical applications.

Another usual strategy for enhancing the sensor response consists of using the so-called fiber-integrated resonators. An immense variety of resonators have been proposed in the literature, obtaining novel fiber-based devices able to increase the sensitivity in the measurement. In this review, examples of whispering gallery mode (WGM) and Fabry–Perot resonators (FPR) are described as representative examples of these fiber-integrated resonators.

WGM resonances have been used for multiple purposes, from strain measurements [91] to optoelectronics components [92]. These systems have also been proposed for chemical sensing, since they have demonstrated excellent sensitivity of the WGM frequencies to RI and long effective path lengths that provide larger analyte–light interaction. For instance, Boleininger et al. developed a WGM sensor based on a pair of crossed standard optical fibers capable of detecting unlabeled biochemical species (streptavidin). In addition, the sensor was fabricated in a cell to carry out measurements in aqueous solutions [93].

Fabry–Perot resonators (FPR) have also been widely used as optical sensors for measuring a variety of parameters such as pressure, strain or temperature. These sensors are created by cut air slots penetrating the core of the fiber, allowing the formation of standing waves in the hole area. Various manufacturing processes have been proposed to create these devices. For example, two polished fiber end faces can be hosted in a holey sleeve, but this assembly is complicated, requiring other materials such as epoxy resins, and also has a strong dependence on temperature [94]. Other more recent approaches consist of chemical etching or laser micromachining [95, 96]. The latter process was employed to create a FPR that is showed in Fig. 6 as an example. These setups have several advantages, such as large dynamic ranges, small temperature dependence and the possibility of accessing liquid samples for direct RI measurement in the microcavity [95]. Also, high sensitivities are obtained through these systems, for example, Wieduwilt et al. proposed a FPR which showed RI sensitivity of about 1.5 μm/RIU [96].

4. The versatility of MOFs. Manufacturing and materials

Having described the main types of fiber based chemical sensors, this section focuses on MOFs, as this fiber is more versatile than SMFs or MMFs. Knight et al. demonstrated the first silica MOF in 1996. In this work, they defined it as "a pure silica core surrounded by a silica–air photonic crystal material with a hexagonal symmetry", and whose physical appearance can be seen in Fig. 7A [97]. Given the exceptional properties of this novel waveguiding material, new approaches have been developed since then. Nowadays, many different types of configurations are possible, making them interesting for chemical sensing and biosensing. This section intends to provide a general overlook of these fibers considering briefly aspects such as the manufacturing, final designs, sensing principles and convenient structures depending on the applications.

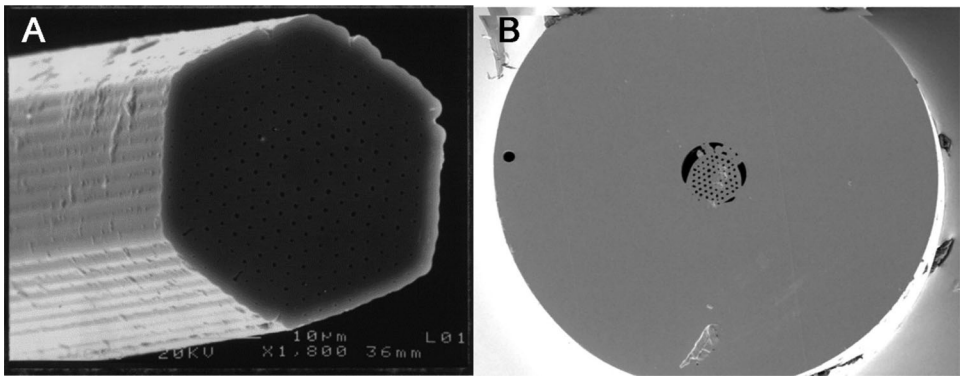

Figure 7 SEM images of the first silica (A) and polymer (B) MOFs reported in the literature. (A) taken from [97] and (B) taken from [99] with permission of The Optical Society.

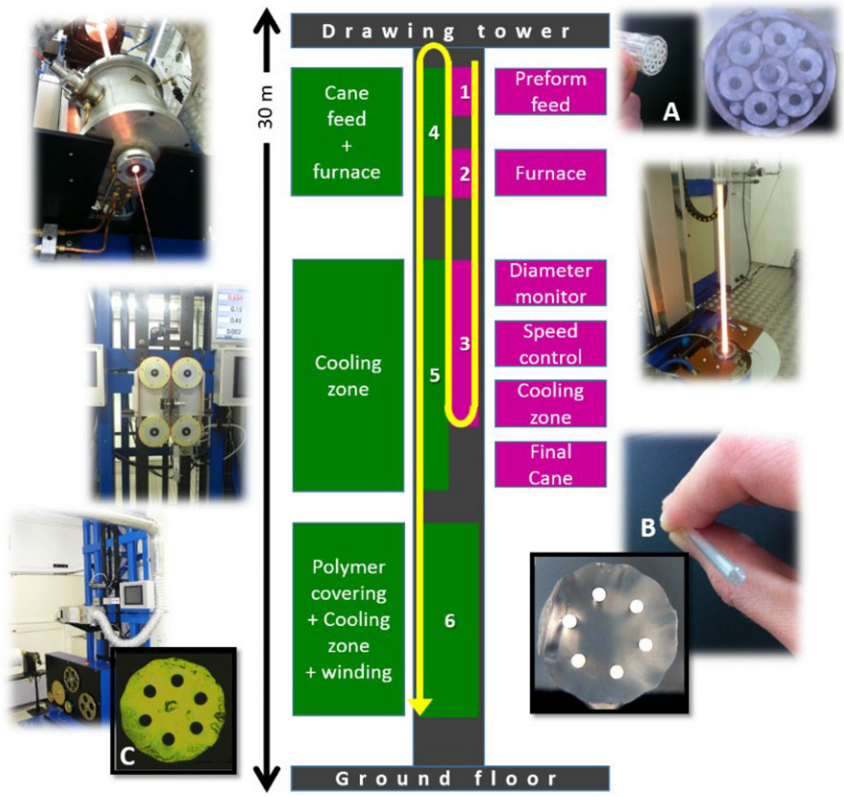

Figure 8 Scheme with illustrative images for the stack-and-draw technique for the fabrication of silica MOFs and microstructures. (A) Silica preform (2–3 cm); (B) Silica cane (2–3 mm diameter); (C) Silica PCF (200–300 μm diameter). Figure adapted from [98] with permission of John Wiley & Sons.

Regarding the manufacturing method, there are different technologies but the stack-and-draw technique is the most employed for the fabrication of MOFs [9, 35]. This methodology can be used as well for the fabrication of microstructured capillaries (MSCs). Figure 8 depicts a scheme of the stack-and-draw technique [98]. In this methodology, a bundle of silica rods and capillaries are stacked, maintaining the final MOF microstructure. After stacking, the preform is fused in the furnace employing temperatures between 1800 and 2200°C (depending on the tower), and the deformable silica is drawn down. Sometimes pressure is necessary to avoid hole collapse. By modifying the feed speed and fiber drawing speed, as well as the pressure and the temperature, different types of MOFs can be obtained from the same preform. Once the glass fiber is drawn, it is coated with a protective coating, usually acrylate or polyimide, in order to make it more flexible and avoid humidity inside the structure.

With materials other than silica, the stack and draw technique becomes less usual. Polymer MOFs are of particular importance in chemical sensing. Polymer MOFs were first manufactured in 2001 by Eijkelenborg et al. Figure 7B depicts the SEM image of this novel polymeric structure. By drilling the poly(methyl methacrylate) (PMM(A) preform, the final fiber could be drawn and studies proved its ability to guide light in single mode [99]. Polymer MOFs can also be obtained starting from a preform manufactured following the extrusion method [35, 100]. The use of a conventional fusion splicer has also been used to manufacture MOFs, allowing the fabrication of novel hybrid polymer–silica structures for different applications [101]. After manufacturing, different modifications

of the structure can be made to enhance the performance of these devices. For example, laterally accessible polymeric MOFs to provide real-time chemical sensing and biosensing and a functionalization of the core without interferences from the cladding has been proposed [102]. The manufacturing of polymeric MOFs with both microstructured core and cladding has been reported, also obtaining an increase in the interaction between the light and the substance inside the fiber [103].

Focusing on the type of material, silica fibers are the most employed, although other materials such as soft glass have been used for chemical sensing. Soft glasses are used in some applications where the wavelengths employed are beyond the transmission windows of the silica glass, such as the infrared region. These materials have been recently employed to fabricate glass MOFs to detect quantum-dot labeled proteins, allowing a limit of detection (LO(D) of 1 nM [104]. As mentioned before, optical fibers can also be made of polymer, PMMA, with their handling easier, but having limitations overall in the temperature range (limits are usually below 100°C and in some cases 200 °(C) [35]. With regard to polymers, PMMA was used to manufacture a SPR sensor based on PCFs and metal nanolayers, obtaining numerical simulation results of 8.3×10^{-5} and 9.4×10^{-5} RIU [105]. When focusing on functionalization of these structures for biological characterization purposes, it seems that polymer MOFs can be chemically modified in a faster way than silica MOFs. However, glass MOFs present benefits regarding biosening, as for example spectral regions such as UV-Visible (UV-Vis) (with high-purity silica glass) or midinfrared (with soft glasses) can be achieved [106]. Also, silica PCFs can be functionalized, for example, by filling specific holes with Ge, acting as micrometer-sized wires to obtain new in-fiber sensors [107]. Finally, another polymeric material, TOPAS cyclic olefin copolymer (CO(C) has been implemented in MOF manufacturing and has shown unique properties: i) contrary to PMMA MOFs, this polymer is humidity insensitive, making it more attractive for chemical sensing [108]; ii) it has lower loss than PMMA at THz frequencies [109] and; iii) it is photosensitive to allow fabricating fiber Bragg gratings into them [110].

There are other designs such as strong penetration PCFs, double-clad PCFs, dual-core PCFs that can improve the interaction between light and matter and decrease the attenuation of the structure [111]. With SC-MOFs and HC-PCFs the most employed for chemical sensing in fluid media, the other structures and types of MOF have also been tested obtaining promising results, as described in Section 5. Depending on the final application and the desired properties of the system, different PCFs are proposed. To give an example, accuracy and periodicity along the structure is less stringent for sensing with SC-PCF than for HC-PCF [112]. Also, if Raman spectroscopy is used as the detection technique, SC-MOFs are more robust platforms compared to HC-MOFs [113], allowing in principle detection sensitivities in the 10^{-10} M range [93].

As previously described, MOFs can be used in chemical sensing due to their practical advantages compared to conventional optical fibers. First, there is no need to remove the coating and the structure is more robust than that from conventional fibers (see Fig. 2) where the coating of fibers is removed), as fluid can be introduced into the holes of the MOFs to carry out the light–analyte interaction. Secondly, the amount of liquid necessary for the detection is smaller than that used in conventional fibers and in classical spectrophotometry glass cuvettes, as volumes in the order of μL are inside the structure [35]. Injection of fluids into MOFs is carried out through different approaches. The easiest mode is filling by capillary action, where the surface tension causes the liquid to fill the capillary. Pressure pumps can be employed to accelerate this process, even from analytical equipment such as high-performance liquid chromatography (HPL(C) or capillary electrophoresis (C(E) [114]. It might be the case that a selective filling is desired, overall when a selective guiding is pursued, as explained below. To this aim, different procedures can be carried out. For example, UV-curable polymers can be inserted in the fiber and a posterior sealing of the cladding can be made, leaving the hollow core open, though this methodology is time consuming [115]. Another alternative consists of the use of a fusion splicer to close the air cladding, whose holes are smaller than that from the hollow and therefore their closing is faster, although it is not a reproducible methodology [101]. New approaches are also described to selectively fill MOFs, such as the lateral access to the holes of PCFs, or the manufacturing of silica exposed-core MOFs. To show representative examples, Fig. 9A depicts an image of a fiber with a lateral access to simultaneously fill the fiber and propagate light from one of the extremes [103]. In Fig. 9B is shown a preform fabricated to produce silica exposed-core fibers [116]. Finally, other novel approaches have been recently proposed, such as the selective filling of MOFs by using ion beam-milled microchannels, a technique that provided robust inline devices and low coupling loss. This technique consists first of milling the microchannel into the end facet of a MOF. Then the MOF is spliced to an SMF, it being possible to fill any pattern of channels. As the splicing process is performed before the material infiltration, contamination of the splicer is avoided [117].

The light–matter interaction within the fiber will depend on the internal structure and the way that the fiber has been filled, i.e. both the internal structure and the RI of the fiber material (silica, soft glass, polymer) and the fluids inside the fiber containing the analyte of interest. The most important difference among these structures is the core, being solid for SC-MOF (Figs. 3A and (B) and hollow for HC-MOF (Figs. 3C and (D). Supposing that $RI_{glass} > RI_{fuid}$ (for example, when filling the fiber with gas or aqueous solutions), the light is confined in the core of both structures and is guided along the structure with very low attenuation, but on the basis of different phenomena. For the SC-MOF the light is guided by TIR through the solid silica core, while for the HC-MOF the light is guided via the photonic bandgap effect through the whole core. When using this strategy, one must take into account that interaction between matter and light for the SC-MOF will be weak and only the substance inside the holes

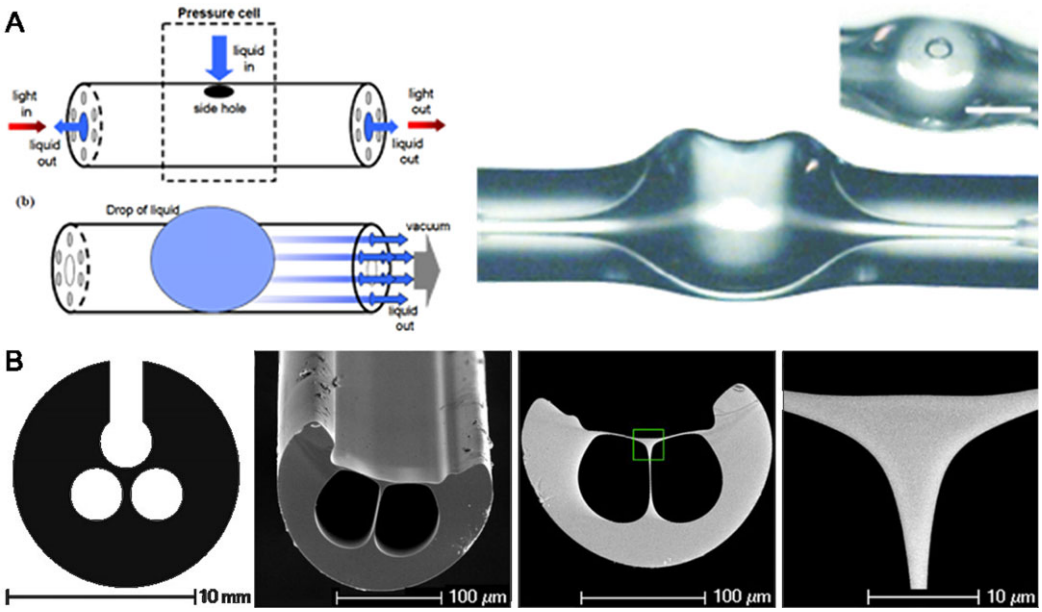

Figure 9 Example of procedures to make a lateral access in a PCF. (A) hole made on the surface of the fiber to fill it with liquid through the lateral access and guide the light from one end of the fiber to the other end (left, scheme, and right, picture of the final fiber with the lateral access). Figure taken from [103] with permission of the Optical Society. (B) From left to right, design, SEM images and enlargement of the core of a silica exposed-core fiber. Figure taken from [116] with permission of the Optical Society.

surrounding the core will interact with the beam inside the core, as the evanescent field zone is the only area where the interaction takes place. On the contrary, for the HC-MOF, as the sample under study is inside the hollow core, interaction with light that is also passing through the core, will be much larger. As RI_{holes} increases, it approaches RI_{glass} and the difference between the RIs decreases. This fact causes a poorer light confinement inside the core for both structures, which will affect the interaction. While this may be advantageous for the SC-MOF because interaction is expanded to the distant holes, the interaction in the HC-MOF will be insufficient. For this reason, when using HC-MOFs for sensing there are two alternatives. The first consists of filling all the holes (cladding and core). Although this filling is simpler, the shifted transmission wavelength of HC-MOF may not match the excitation wavelength, and therefore light is hardly guided and is not confined into the core region, providing a low light–matter interaction. The second alternative, consists of sealing the cladding, achieving a higher light confinement in the core, as the RI of the cladding remains lower. Nevertheless, this methodology is more complicated and time consuming [118]. Another possibility is the use of liquids with similar RI to that of the fiber material. In this case TIR is achieved for both structures and interaction between light and matter appears in all the holes of both types of MOFs. However, the RI of aqueous solutions is usually lower than that of silica and other fiber materials and therefore TIR does not appear in biological and medical assays [35, 102].

Considering the above-mentioned sensing strategies, the following section will cover some relevant applications of PCFs in chemical sensing and biosensing. This section is organized in subheadings according to the type of structure employed in each case. Within each subheading, articles are described chronologically and as a function of the detection principle used.

5. Sensing applications with MOFs in fluid media

5.1. Sensing with SC-MOFs

This section includes the most relevant works focused on the use of SC-MOFs in chemical and biochemical sensing during the last ten years. From the literature, both fluorescence detection and Raman spectroscopy have been the most employed detection systems. However, UV-Vis absorption, RI measurements and changes in the wavelength shift have also been employed to detect molecules in fluid media.

Regarding fluorescence detection, Konorov et al. tested various fused silica and soft glass PCFs to detect a dye (thiacarbocyanine). This sample was selectively injected in the cladding of the PCFs by a capillary array. The fluorescence signal from the dye was then collected in the cladding, whereas the irradiation was induced in the core of the PCFs. This strategy showed promising results in the analysis of thiacarbocyanine, but only worked efficiently when the RI of the liquid medium exceeded the RI from the glass. In addition, the protocol proposed was also valid for implementation in microchip technologies [118]. Cordeiro et al. proposed a new methodology to selectively fill SC- and HC-PCFs (see Fig. 9(A)). In the case of the SC-PCF,

the opening of the cladding was not reproducible. For both structures, the lateral filling with rhodamine was achieved and this substance was successfully detected [119]. Other fluorescent dyes such as fluorescein have been detected through SC-PCFs. Williams et al. employed a SC-PCF of 30 cm length and 500 nm core diameter to measure the fluorescence of fluorescein in nM concentrations. As interaction of light was only evidenced in the walls of the holes, a replacement from run to run was more convenient to avoid contamination between analyses. LODs of 0.3 nM for the SC-PCF were obtained [121].

Not only silica SC-PCFs, but also polymer SC-PCFs have been used for fluorescence detection in fluid media, though to a lesser extent. This fiber type presents high interest in biological applications due to its biocompatibility. As an example, Jensen et al. detected antibodies in a SC-PCF made of polymer of 20 cm length, 300 μm external diameter and a silica core surrounded by 6 big holes of 60 μm diameter. Detection of Cy3-labeled antibodies α–streptavidin and α-C-reactive protein (CRP) was based on the interaction of light from the evanescent field generated in the surrounding zones of the core. The fluorescence radiation for detection covered 7 cm of the total fiber length. The procedure to make the antibodies detectable in the sensor was achieved in 6 steps, compared to the 10 steps necessary in silica structures. LODs of 80 nM in sample volumes of 27 μL evidenced the excellent sensitivity obtained [122].

The use of PCFs for Raman spectroscopy is a recent trend in chemical and biochemical sensing applications due to the advantages of both technique and detection platform. As Raman spectroscopy is a powerful optical technique for chemical and biochemical analysis, the signal generated is extremely low compared to other optical detection techniques such as fluorescence. The use of PCFs as platforms for Raman spectroscopy is becoming increasingly attractive as this structure provides high sensitivities, specificity and versatility. Raman spectroscopy probes have been tested in both SC-PCF and HC-PCF, the latter being more suitable as the sample is introduced in the central hole and the confinement of light in the center makes the light–analyte interaction larger, thus Raman signal increases. Pristinski and Du demonstrated the use of a SC-PCF (OFS Laboratories, Somerset, NJ) as a Raman spectroscopy platform. The fiber employed consisted of a 2.5-μm core diameter surrounded by 126 air holes of 3.5 μm diameter. Acetonitrile was introduced in the SC-PCF using a custom high-pressure vessel at 200 psi. Instead of removing the silica background signal, the authors employed it as a reference. Peak ratios from the silica core and acetonitrile contained in the air channels did not vary with the laser power or fiber length. Dependence on the laser power was negligible with the fiber length, and a linear relationship was obtained for the Raman signal versus fiber length [113]. Amezcua-Correa et al. applied silica SC-PCF for SERS measurements. Fibers of 15 mm length were used in the sensing system. The internal walls of the holes inside the fiber were coated with Ag nanoparticles by the high-pressure chemical deposition technique. This technique allowed a controlled deposition of nanoparticles, creating a robust template to enhance the SERS signal. This,

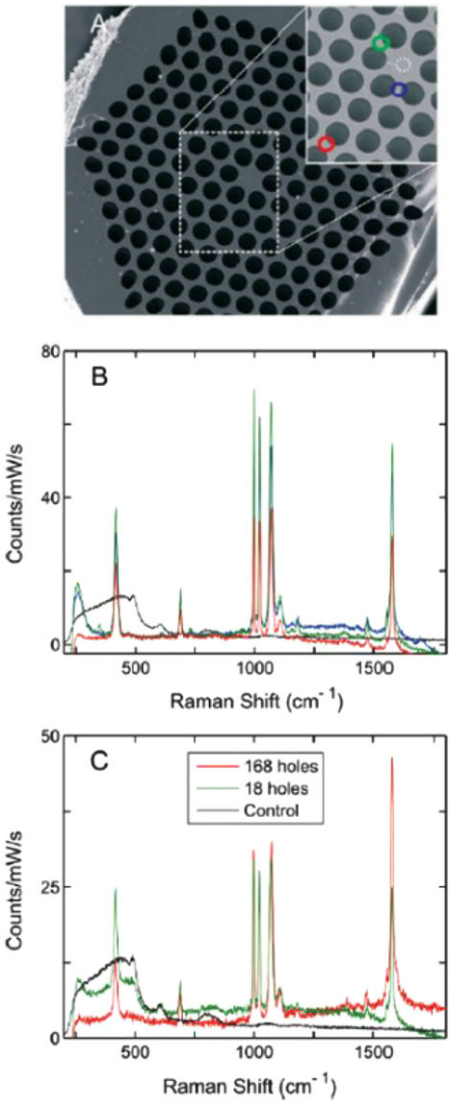

Figure 10 (A) SEM image of the SC-PCF employed for SERS detection. (B) SERS spectra according to the colored areas marked in the SEM image. (C) Comparison of the SERS spectra obtained from the 168- and 18-hole structures, irradiating the beam in the core of the structure (black spectra corresponds the SERS spectra with no Ag nanoparticles filling, taken as control). Figure taken from [92] with permission of John Wiley & Sons.

combined with the advantages of long-path interaction of PCFs, provided the increase in intensity of benzenethiol as analyte under study. In Fig. 10A a SEM image of one of the structures employed (168 holes), as well as the SERS signal from the silica (Fig. 10(B)) are depicted. In Fig. 10C benzenethiol Raman spectra from the 168-hole, 18-hole and the control without Ag nanoparticles were compared, evidencing the enhancement of signal when Ag nanoparticles were previously deposited [66]. Xie et al. also designed a SERS sensor using a silica SC-PCF and silver nanoparticles, being useful in both the visible and near-infrared regions. Detection of 4-mercaptobenzoic acid was fulfilled in the range of mM concentrations. The strategy followed, contrary to

previous works where the high-pressure chemical deposition is employed, consisted of filling only 1 cm of fiber with Ag nanoparticles solution by capillary action. Compared to the signal obtained without Ag nanoparticles, high intensities were obtained, in addition to a good reproducibility of the results [123].

Finally, other measurements have been used for chemical sensing with SC-PCFs. For instance, detection based on UV-Vis absorption has been successfully achieved through SC-PCFs. Martelli et al. proposed the use of a pure silica SC-PCF to detect porphyirin in water solutions. After filling the SC-PCF of 22 cm length with an aqueous solution containing the sample by capillary action, which took 3 h, the detection was performed by using an excitation laser at 640 nm and detected with an optical spectrum analyzer [124]. Rindorf et al. developed a glass SC-PCF long-period grating for biochemical sensing. This study showed the first label-free technique to detect biomolecules, by taking a PCF of 30 cm length. The system was robust, and did not require calibrations, being also insensitive to temperature fluctuations. The PCF had 168 holes and a pitch of 7.2 μm. LPGs were inscribed with a nondestructive CO_2 laser method. First, hydroxyl groups were created on the inner surface of the holes and a layer of poly-L-lysine was then attached in order to create positive charges. Then, deoxyribonucleic acid (DN(A), which possesses negatively charged phosphate groups, was attached to the poly-L-lysine. Both monolayers had similar RI to that of silica (of the order of 1.453 at 850 nm) and therefore the evanescent wave-sensing principle was used to detect the monolayers. The resonant wavelength of the grating inside the holes was increased when depositing the different layers. On the basis of the wavelength shift, the authors were able to measure the thickness of the biofilms, being 4.79 nm for the poly-L lysiene and 1.65 nm for the DNA layer [125]. Finally, it is important to highlight that other physical properties from liquids, such as the RI of the solutions, can be employed for chemical sensing. As an example, Wang and Tang developed a Mach–Zehnder interferometer by fusion of a section of PCF (LMA-10, Blaze Photonics) between two standard single-mode fibers. The RI of different sucrose solutions ranging from 1.333 to 1.422 was measured with resolutions of 1.62×10^{-4}–8.88×10^{-4} RIU for sensing length of 3.5 cm, and 1.02×10^{-4}–9.04×10^{-4} RIU for a sensing length of 5 cm. The PCF interferometers were stable to environmental changes in temperature [126].

It is important to mention other subtypes of SC-MOFs such as suspended-core MOFs, that are gaining popularity in fiber-based chemical sensors. In fact, a specific review with the most important applications concerning this type of fiber was recently published [127]. These structures have also demonstrated enhanced sensitivity compared to the detection in traditional cuvettes, allowing the quantification of analytes, such as $NiCl_2$ in aqueous solutions [128]. For instance, Ruan et al. employed a soft glass MOF to deposit a layer of antibodies in the inner walls of the holes. First, the internal surface was cleaned to remove debris and create hydroxyl groups, then a silanization of the internal surface and a crosslinking layer were formed to connect the silane layer with the antibody. To detect the antibodies, these were attached to quantum dots (Qdot800 and Qdot705). In order to select the material for fiber fabrication, an antibody at 100 nM was used as standard for fluorescence performance in different types of glass. The F2 glass MOF was made with 1.3 μm core diameter and approximately 9 μm hole diameter for a fast filling. The protein used for immobilization was the Qdot 800 goat F(ab')2 anti-mouse IgG conjugate. A confinement loss was evidenced after immobilization (from 2 to 30 dB/m, and only short-length fibers between 19 and 25 cm were employed for fluorescence measurements). The results showed that the fluorescence signal was dependent on the surface antibody density in the inner walls of the holes [106]. Emiliyanov et al. designed and fabricated a polymer suspended-core MOF made of TOPAS COCs. This polymer is not only biocompatible but it also avoids the problem of bubble formation during the fabrication process of MOFs of other polymeric materials such as PMMA. The structure consisted of a suspended-core MOF with three big holes of 50 μm diameter, core diameter 12 μm and 220 μm outer diameter (O(D). Antraquinone molecules were first attached to the inner surface of the holes to facilitate the binding of these biomolecules. The selective detection of antibodies was also tested and confirmed by detection of two analytes (α-streptavidin and α-CRP). These biosensors need an extra biolayer to be functionalized with biomolecular capture layers [129]. However, this extra layer can be employed to create biomolecular sensors in series, such as the system proposed by Emiliyanov et al. who created the first biosensor capable of sensing several anti-body biomolecules in series along the same MOF [24]. Yan et al. demonstrated the use of a suspended-core MOF with four air holes between the solid silica core and the photonic crystal cladding holes, which allowed a large sample volume inside the structure. The central core was a rectangle of 10×6 μm, the 4 big holes had a diameter of 20 μm, while the surrounding small holes had an average diameter of 2.5 μm, with the total diameter of the fiber 300 μm. Compared to HC-PCF, this structure can be used at different excitation wavelengths due to their index-guiding nature. In this study, the suspended-core MOF was liquid filled by the capillary effect, while Au nanoparticles (80 nm) were previously deposited on the inner walls or mixed with the sample solution. 5 cm of fiber were cut and a sample of rhodamine B 1×10^5 nM was employed as the analyte probe, introducing it by the capillary effect after deposition of Au nanoparticles. The Raman spectrum of rhodamine B in the MOF probe was identical to that from a silicon wafer coated with the same Au nanoparticles. The Raman intensity did not vary on removing the coating of the fiber. On the other hand, a solution of rhodamine B mixed with Au nanoparticles was introduced in the system for comparison with the previous experiment. The same spectra was obtained in this case, but lower concentrations (100 nM) were detected, as the mixture allowed Au nanoparticles to interact more effectively in the whole solution. The theoretical results corroborated an evanescent field yield with values of around 21.5% [130]. Ott et al. employed a SC-PCF to carry out the detection process of biomolecules attached

to the walls of the holes in the fiber. This detection was performed inside this fiber through a change in the modulational instability gain spectrum caused by the selective capture of the biomolecules under analysis. The setup proposed provided label-free sensing with sensitivities approximately 7.5 times higher than the previous label-free MOF biosensors reported in the literature [131]. Later, in 2011 Frosz et al. achieved the highest sensitivity experimentally demonstrated for aqueous solutions by using MOFs with enhanced nonlinearity [132].

5.2. Sensing with HC-MOFs

This section deals with the most relevant works on the use of HC-MOFs as sensing platforms. As well as for the SC-MOF, fluorescence detection and Raman spectroscopy have been the detection techniques employed in these systems. Note that HC-PCF can guide light without leakage using the photonic bandgap effect, as explained before. This phenomenon can be used for other interesting applications apart from fluorescence and Raman sensing, such as particle guiding. Benabid et al. successfully performed the levitation and guidance of a polystyrene particle inside a HC-MOF through 150 mm and with a speed of 1 cm s^{-1}. Biological, chemical and engineering applications are increasingly employing this strategy to guide particles inside objects with minimal dimensions or where noninvasive analysis are required [133].

Focusing on fluorescence measurements, Cordeiro et al. detected rhodamine in SC- and HC-MOFs by employing a new methodology to selectively fill the MOFs. Since no contact with the fiber extremes is needed, sample introduction and optical alignment are independent, which is of great advantage for using in an optical sensing in laboratories [103]. Smolka et al. also compared a SC-MOF and a HC-PCF for absorption and fluorescence sensing. The inhouse SC-PCF was Ge doped, cladding holes of 3.7 μm diameter, and a core of 19 μm were used. In addition, 7 holes with reduced diameter were introduced in the core to enhance the light–matter interaction . An evanescent field between 0.4% and 1% was estimated. The HC-PCF with cladding holes of 1.45 μm diameter and core of 5.3 μm (from Crystal fiber, HC-532-01) was selectively filled in order to guide light in the core and achieve from 92 to 99% of evanescent field yield, providing a larger light–matter interaction than with the SC-PCF. Concentrations down to 5×10^{-8} and 1×10^{-10} absorbance units (AU) were detected in absorption and fluorescence measurements, improving the detection by 4 orders of magnitude compared to previous systems [134]. Shinoj and Murukeshan employed two different silica HC-PCFs to detect fluorescent microparticles. On the one hand, two different media (water and ethanol) were pumped into the structures. On the other hand, two different structures using the same medium were tested in order to compare the fluorescence collection efficiency. Solutions with the sample were introduced by capillary action. The fluorescence response was found to be more efficient when

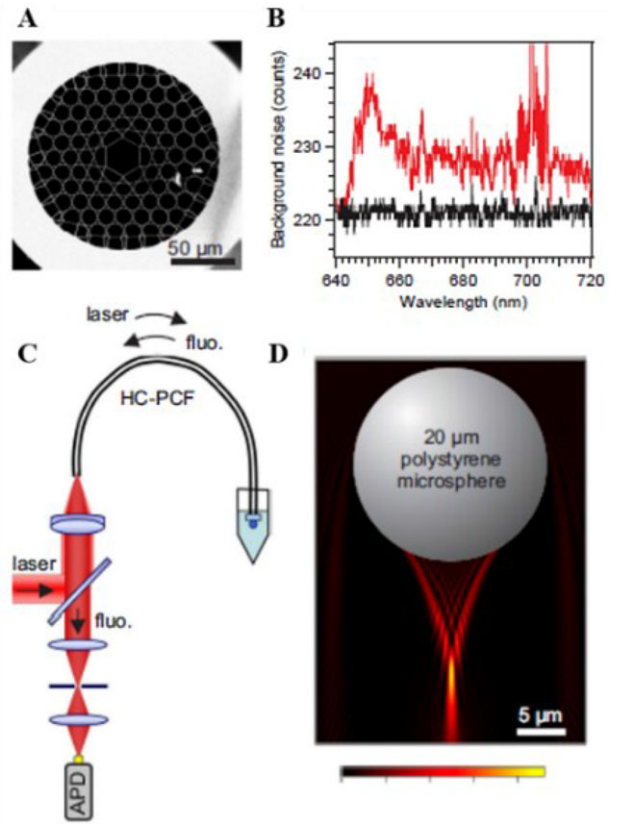

Figure 11 (A) SEM image of the Kagomé-lattice HC-PCF. (B) Luminescence background spectrum (red) with maximum 11 mW input power and 10 s integration time (the black line is the background noise of the spectrometer). (C) Experimental setup. (D) Computed electric field intensity with a 10-μm polystyrene sphere illuminated by the fundamental Gaussian-shaped fiber at a wavelength of 633 nm. Figure taken from [137] with permission of The Optical Society.

using water as medium, as well as the structure with central wavelength of 1060 nm [135]. The same authors also proposed an integrated HC-PCF transverse optical trapping system for optical manipulation and detection. Taking advantage of the high sensitivity of fluorescence detection and the high light confinement in HC-PCF the authors were able to detect biological samples by immobilizing them on the walls of the core of a HC-PCF [136]. More recently, Ghenuche et al. demonstrated the improvement in signal-to-noise ratio and a 1000 $\times$ reduction of the LOD by using a Kagomé HC-MOF (Fig. 11(A)) for fluorescence sensing. A remote system was designed and developed, as can be seen in Fig. 11C. To achieve these improvements in the detection, a 20-μm polystyrene microsphere was employed as a focusing lens. The production of this beam through dielectric microspheres is known as a photonic nanojet and provides excellent optical properties for some applications. Figure 11D shows the nanojet and microsphere employed in the system. Fluorescence correlation spectroscopy (FCS) was employed in this study to analyze the fluorescence signal. Thanks to the microsphere probe, the noise (1.2 kHz)

was about 40 times lower than previous works (270 kHz). In Fig. 11B the background signal of the system is showed. LODs of 0.4 nM were obtained, 1000 times lower than previous systems, in volumes of approximately 6×10^{-9} μL. In addition, as a proof-of-concept, the differentiation of two dyes with similar fluorescence (Alexa fluor 647 and Cyanine Cy5 attached to a protein Annexin A5b) was achieved thanks to their different diffusion properties through FCS analysis [137]. Kagomé lattices have also been used to detect dyes such as fluorescein. Williams et al. employed a Kagomé HC-MOF of 30 cm length with core diameter 19 μm to measure the fluorescence of fluorescein in attomole amounts and achieve LODs of 0.02 nM. The HC-MOF was flushed between runs, and contrary to SC-PCFs, no replacement of the structure was required [121].

As previously noted, the use of fibers for Raman and, specifically SERS, has gained attention during last years. Yang et al. collected the most important articles concerning the use of fibers such as HC-PCFs, liquid core PCF (LC-PCF), inner-wall-coated LC-PCF, liquid-filled HC-PCFs and modified highly sensitive LC-PCF for SERS probes [68]. However, in the present review, only the most recent studies on HC-PCFs for SERS and Raman spectroscopy systems are discussed.

Yan et al. employed a HC-PCF of 8 μm core diameter, 2.5 μm holes, 100 μm OD for SERS measurements, depositing Au nanoparticles in the inner walls of the holes. Fibers of 5 cm length were taken and a colloid of Au nanoparticles of 100–200 nm was introduced by capillary action (1–3 cm), after drying at 60 ºC for 2 h, rhodamine B solution was introduced, and was also dried. Signals from the analyte were verified after subtracting the background spectra from the silica. Irreproducible results were attributed to irregularities in the fiber structure [69]. Not only Au but also Ag nanoparticles have been employed to enhance Raman signal in HC-PCF. Zhang et al. employed a HC-PCF to develop a fiber sensor based on SERS scattering. The commercial fiber employed (Crystal fiber, model Air-6-800) was selectively filled in the core (previous sealing of the cladding), in order to maintain the bandgap and confine light in the hollow-filled region. Due to this strategy, a higher light–matter interaction compared to previous works was evidenced. A fiber of 10 cm length was cut, selectively filled by capillary action during 5 s in order to introduce 1 cm of sample with Ag nanoparticles (ranging from 40 to 60 nm diameter). Spectra of rhodamine 6G, human insulin and tryptophan were obtained by using the fiber as Raman platform. The latter analyte was also detected through a dry film for comparison, and an estimated enhancement factor of ~100 was obtained for the HC-PCF [70]. In order to obtain a higher increase in Raman sensitivity, the use of various layers of nanoparticles has been proposed. Shi et al. developed a sensor based on a double substrate surface to enhance SERS. Two different structures were tested, a HC-PCF (Thorlabs, model HC-633-01) and a hollow silica waveguide (HSW). The HC-PCF (after sealing the cladding to fill only the core) possessed a better light confinement and hence a higher sensitivity. However, the core (5 μm) was too small to make a correct coupling with the laser beam. The HSW (a capillary tube from Polymicro Technologies) presented a larger hole (300 μm), and light coupling was much easier, although a loss in confinement was expected. By the deposition of two layers formed by two different types of Ag nanoparticles, an increase in sensitivity was observed, compared to previous methods with only one layer. For both structures the first Ag layer was deposited on the inner surface of the core, whilst the second type of Ag nanoparticles was mixed with the sample solution and introduced into the core by the capillary effect. Regarding the HC-PCF, the strongest SERS signals were obtained when measuring the analyte by positioning the laser on the sealed end of the fiber (which gave an intensity 100 times higher than a direct sampling in a glass cuvette). The shape of the sealed end (concave) could be a reason for this enhancement, compared to the detection from the open end (10 times lower intensity). Focusing on the HSW, an intensity 5 times higher than the direct sampling was obtained, being in addition a low-cost alternative to HC-PCFs, although less sensitive. Figure 12 shows the Raman spectra of the analyte (rhodamine 6G) where the comparative of the signal with the HC-PCF against a glass cuvette in (A), as well as the HSW improvement respect to direct sampling [71].

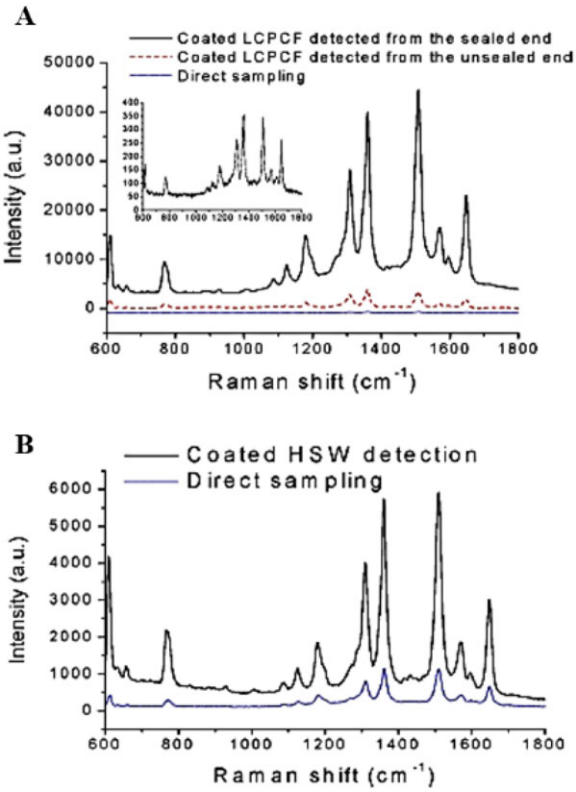

Figure 12 Rhodamine 6G spectra at 1000 nM by using different methods: (A) comparison of direct sampling to coated LC-PCF; (B) comparison of direct sample and coated HSW. Figure taken from [71] with permission of American Institute of Physics.

As well as dyes such as rhodamine, other more complex molecules have been detected by using SERS and

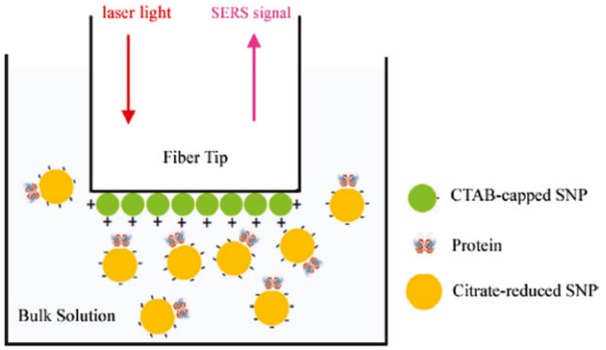

Figure 13 Scheme of the "sandwich" proposed by the authors for SERS sensing of proteins with a MMF (SERS: surface-enhanced Raman spectroscopy; CTAB: cetyltrimethylammonium bromide; SNP: silver nanoparticle). Figure taken from [72] with permission of ACS Publications.

HC-PCFs. Yang et al. detected proteins and bacteria in aqueous solution by using tip-coated MMFs and HC-PCF through SERS. Proteins lysozyme and cytochrome c as well as the bacteria *shewanella oneidensis* MR-1 were detected in aqueous solutions obtaining improvements in sensitivity compared to previous works. Two different systems were employed. A tip-coated MMF was charged positively with Ag nanoparticles and proteins mixed with other negatively charged Ag nanoparticles were introduced, creating a "sandwich" scheme with two different types of Ag nanoparticles. Figure 13 depicts a scheme with the "sandwich" and the system proposed by the authors. Concentrations as low as 0.2 mg mL^{-1} were obtained with this system, one order of magnitude lower than a direct measurement with a glass cuvette. The second approach was based on the use of a HC-PCF with the cladding sealed to confine light in the core (6 μm diameter), filled with the bacteria under study, obtaining LODs of 10^6 cells/Ml [72]. Dinish et al. employed a HC-PCF for SERS detection of cancer proteins in low sample volumes. The fiber of 8 cm length had a core diameter of 9.5 μm and cladding of 135 μm (from NKT Photon. HC 800–01), and it was cut and cladding sealed. Epidermal growth factor receptor (common biomarker for a variety of cancers) was immobilized on the walls of the core and Au nanoparticles were attached for SERS measurements. After immobilization of proteins by capillary action SERS experiments were carried out, obtaining intensities one order of magnitude higher than those from the traditional material (glass slide). By introducing extremely low volumes, in the order of nL, amounts of approximately 100 pg of cancer protein were detectable, which increased the sensitivity compared to other methods previously reported in the literature [73].

Taking advantage of using HC-PCFs as Raman spectroscopy platforms, the use of Raman measurements without the addition of nanoparticles has also been proposed. This avoids previous steps to adhere nanoparticles for SERS detection. For instance, Khetani et al. were able to monitor the heparin concentration in serum. By matching the excitation wavelength to the wavelength transmission of the filled HC-PCF. A strong interaction of the analyte with the light was achieved, increasing the signal intensity. The fiber geometry was simulated to ensure the shift at the laser wavelength (785 nm). Finally, the commercial HC-PCF with a core size of 10.6 μm and pitch 4.1 μm (from NKT photonics, model HC-1550-04) allowed the shift at the desired wavelength. Background signals from serum were first obtained and a subtraction of its signal was necessary to obtain the Raman spectra of heparin. By modifying the total length of the HC-PCF, a linear relationship between Raman signal and length was evidenced in the range 1–8 cm and a saturation of the signal was obtained for lengths larger than 9 cm. Finally, the quantitative analysis of heparin in serum was carried out, using different standards ranging from 12 to 20 000 United States Pharmacopea units per ml (USP/mL) and a HC-PCF of 5 cm length. A LOD of 10 USP/ml was obtained (within the clinical level detection of heparin in patients during surgeries). Figure 14 shows the Raman measurements of the heparin solutions and the response in intensity as a function of the heparin concentration, providing a linear relationship [120]. Yang et al. developed a glucose biosensor based on HC-PCF and Raman spectroscopy. A HC-PCF of 8 cm length (from Crystal Fiber, model AIR-6-800) was employed in the system. A sample with D-glucose was introduced by capillary action, and one end of the piece of HC-PCF was sealed. Peak signals from D-glucose were in accordance with the direct analysis using a glass cuvette, and the intensity was increased approximately 140 times. Solutions with different D-glucose concentrations were also prepared and measured, achieving detections up to 1 mM [138].

5.3. Other promising MOFs in sensing applications

This section describes studies on chemical sensing in liquid media by using other MOFs as well as other related microstructures proposed in sensing systems.

Strong penetration PCF (SP-PCF) are fibers whose geometry allows a larger evanescent field penetrating into the surrounding holes of the core and increasing the light–matter interaction. In appearance they are similar to HC-PCFs, but the hollow core is not used to carry out the analyte–light interaction, with the structure more similar to a group of suspended-core MOFs connected with silica bridges. Figure 15 shows an example of this type of fiber. Jensen et al. produced a sensor for the detection of biomolecules in aqueous solutions based on this structure. By a correct selection of lattice pitch and air-hole diameter, a large fraction of optical field propagated through the holes interacting with the matter inside them. In this study, Cy5-labeled DNA molecules were detected. Air holes with 3.4 μm diameter were arranged in a triangular lattice with 4 μm pitch. With this design, the central hollow core represented a dead volume, as light–matter interaction was in the holes conforming the lattice. Theoretical calculations

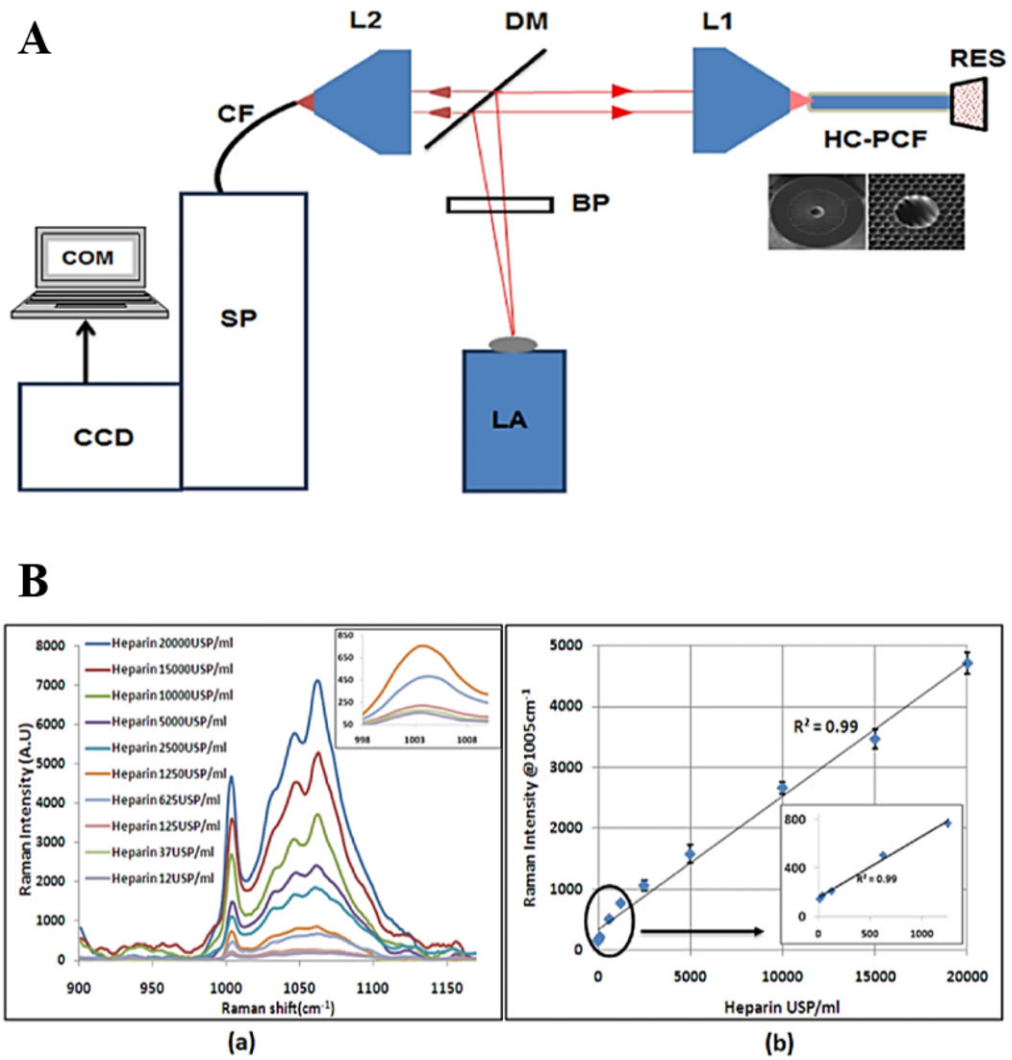

Figure 14 (A) Scheme of the system proposed in [120] (LA: laser; BP: bandpass filter; DM: dichroic mirror; L1 microscope objective lens for light coupling; HC-PCF: hollow core photonic crystal fiber; RES: reservoir; L2: microscope objective lens for backward light collection; CF: collection fiber; SP: spectrograph; CCD: CCD camera; COM: computer). (B) Raman spectra of heparin at different concentrations and peak intensity as a function of the concentration of heparin. Figure taken from [120] with permission of The Optical Society.

estimated a yield in the evanescent field of 5.2%. Then, the air holes were filled with the aqueous solution containing the sample, by capillary action or applying determined pressure, spending around 10 min to fill 20 cm length of the fiber. Concentrations of 5000 nM of Cy5-labeled DNA solution were detected [139].

Defected-core PCFs (DC-PCFs) are other type of MOFs that have proven to be efficient devices in chemical sensing in fluid media. These structures are SC-PCF with some defects in the core made on purpose to enhance the light–matter interaction. Yu et al. used a defected-core PCF made of silica to detect $CoCl_2$. This core consisted of a hole smaller than those from the cladding. Evanescent absorption was studied as a function of the fiber length and analyte concentration, obtaining in both cases linear correlations. A light intensity of 0.37% (of the peak) in the central hole was theoretically estimated, which compared to the 0.03% in the surrounding holes of conventional SC-PCFs for aqueous solutions, was an important increase for sensing applications. By filling the DC-PCF by capillary action with the analyte solution, concentrations of $CoCl_2$ from 0.01 to 0.5 M were detected and a good linear response was obtained [112]. Park et al. proposed a DC-PCF, in this case a GeO_2-doped high-index ring in the center. The use of a doped core allowed a higher evanescent interaction as well as lower confinement loss and splicing loss than previous studies on defected core PCFs without doped ring [140]. Finally, although less employed, DC-PCFs can be used to detect molecules in gas media, such as acetylene [141].

Double clad-PCFs are MOFs that, when combined with gradient-index lenses**,** can guide excitation through

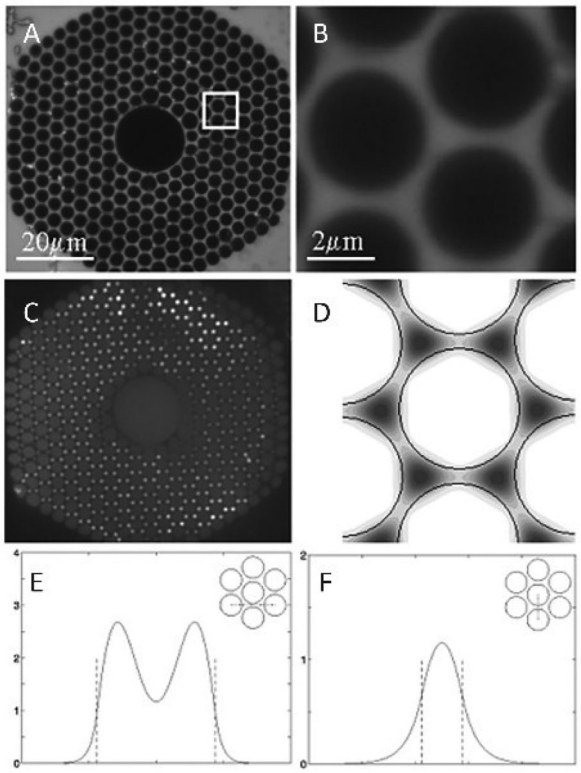

Figure 15 Example of a strong-penetration PCF. (A) Micrograph of the microstructured part of the SP-PCF; (B) close-up where the group of holes is similar to a group of suspended-core PCFs; (C) micrograph of the entire fiber with illumination from the opposite fiber end; (D) field distribution in the sample-filled fiber; (E, F) mode-field profiles calculated along the dotted lines shown in the respective insets. Figure taken from [139] with permission of The Optical Society.

the inner core while light collection can be made through the multimode region. This allows two-fold benefits: first, the input light can show higher intensity for light–matter interaction; secondly, the collection of light is made with a higher aperture, allowing for more efficient photon capture. Knorr et al. employed a double-clad PCF for tissue microendoscopy. Fluorescence lifetimes obtained for the analytes under study were in accordance with the previous literature. Thus, dye standards (RhB, Rh6G and C30) showed a monoexponential decay. However, the behavior of the remaining samples under study depended on environmental conditions. Finally, additional measurements were carried out on fresh muscle tissue, cartilage and tendon samples, following a multiexponential decay, also in agreement with the literature [142].

Dual-core PCFs are structures similar to SC-PCF, but possess two distinguished cores separated by a specific distance. Figure 16 shows a SEM image of this kind of microstructure, which has excellent sensitivity in biochemical sensing applications. Markos et al. investigated this dual-core polymeric MOF to selectively capture antibody molecules by depositing an immobilized antigen layer on the hole wall. By increasing the distance between the solid cores, the sensitivity of the system was increased [143]. These fibers have also been employed for RI sensing of fluids, for instance, Town et al. modified the coupling between coupled cores obtaining advantages such as larger RI measurement ranges and a sensitivity that depended on the fiber parameters [144]. The same strategy was proposed by Yuan et al. who developed a RI sensing system in a photonic bandgap fiber, where one hole acted as analyte carrier and modified the coupling between the cores, obtaining also large dynamic ranges and high RI sensitivity [145].

Multihole capillaries are another type of emerging structures in chemical-sensing devices. They are similar in structure to MOFs, however, their designs are made for sensing purposes only, and thus the guiding principles of optical fibers are not the key parameters in these structures. However, the advantages of their internal structures, similar to MOFs, are employed for high surface-to-volume ratio compared to traditional systems, minimal sample introduced, or low diffusion of the samples. Aouani et al. designed a bundle consisting of 6000 individually cladded optical fibers, 50 cm in length, in which polystyrene microspheres were deposited in one of the extremes for remote FCS. Alexa Fluor 647 was employed as analyte probe. The intrinsic background fluorescence limited the LOD to 400 nM [146]. Guo et al. employed multihole capillaries as platforms for ultrasensitive optofluidic SERS detection. Metallic nanoparticles were inserted into the wall of the inner holes, and two configurations were proposed. Figure 17A depicts the schemes of both designs. The first, based on transversal detection, and the second on longitudinal detection. The transversal-detection configuration provides inline SERS detection for real-time measurements, whereas the longitudinal-detection configuration accumulates the Raman signal along the capillary obtaining high sensitivities. Contrary to the longitudinal detection in HC-PCF, where only the sample injected in the core interacts with the confined light from a laser, in a multihole capillary there is no light confinement and therefore each channel can act independently, increasing the surface area. In addition, all wavelength can be used as there is no need for light confinement. Comparing these structures to SC-PCF, a higher light–matter interaction was achieved, as for the SC-PCF most of the light is confined in the solid core and only the evanescent field interacts with the aqueous sample from the surrounding holes of the microstructure. Finally, short lengths were necessary for the multihole capillaries (∼3 mm) compared to PCFs (usually tens of cm). A multihole capillary with 2700 channels and 117 nm of gold nanoparticles was employed to detect rhodamine 6G molecules, obtaining LODs of 1×10^{-5} nM. Au nanoparticles were introduced using polyelectrolyte mediation, and enhanced the sensitivity in a factor over 10^6. Figure 17B shows Raman signals obtained from both designs developed. LODs of 7×10^{-6} nM for the transversal configuration and 1.4×10^{-6} nM for the longitudinal one were obtained, reflecting the excellent sensitivity of these systems for chemical sensing [63]. The same authors also fabricated, characterized and demonstrated an optofluidic Fabry–Perot cavity sensor with integrated flow-through

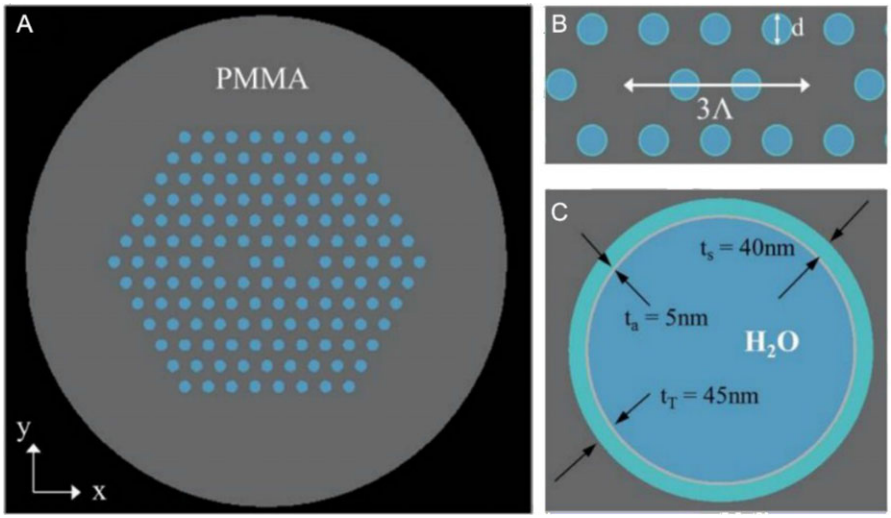

Figure 16 Example of a PMMA dual-core MOF (A), in which the distance between cores is 6 μm and hole diameter of 1 μm (B). In (C) the attached layer of biomolecules inside the holes of the MOF is showed. Figure taken from [143] with permission of The Optical Society.

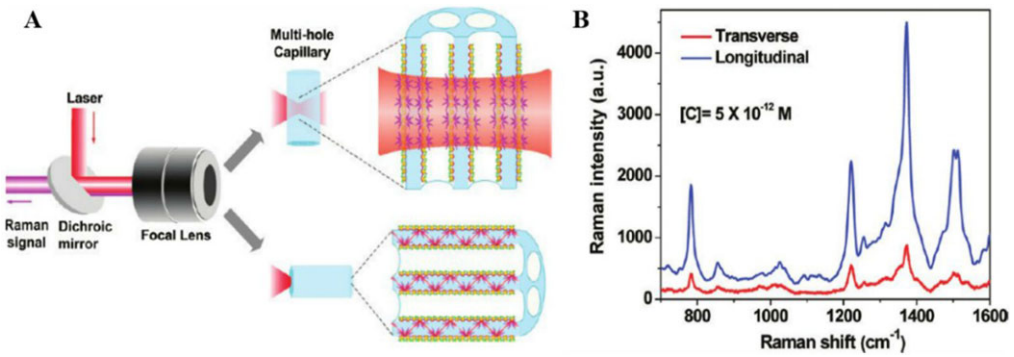

Figure 17 (A) Schemes of transversal and longitudinal detection systems. (B) Raman signals of rhodamine 6G obtained by using the two schemes proposed by the authors. Figure taken from [148] with permission of ACS Publications.

micro/nanofluidic channels. Advantages of this design are the tridimensional detection, which enhances the sensing performance. Two different capillaries with 7000 holes were manufactured using borosilicate glass. The first with 200 μm OD and a hole diameter of 1.8 μm; the second with 90 μm OD and a hole diameter of 650 nm. Pieces of 6 mm were cut for the cavity sensor. Biomolecules attached to the surface of the holes were measured. Changes in resonance (0.37 nm) were evidenced when flushing with the sample containing the analyte of interest (sulfo-NHS-LC-LC-biotin) [147].

5.4. MOFs and microstructures as sensing platforms in conventional analytical instrumentation

Throughout this review different applications of PCFs have been described. Many different designs have been proposed for fluorescence or absorption detection, Raman spectroscopy, or RI sensing. However, the implementation of these structures in analytical instrumentation, and more specifically in commercial equipment, still remains a challenge. For this reason, in this final section some of the works focused on the implementation of these structures in home-made instrumentation, microchip technologies and even commercial equipment are discussed.

Rindorf et al. implemented MOFs fiber sensors in a biochip prototype, allowing the continuous flow of samples along the microstructure and their optical characterization. Figure 18 shows a picture of the system proposed as well as a scheme with the principal components in the sensing area of the system. A commercial fiber (Air-15-1550-MOF) of 125 μm OD, with a centre hole of 17 μm and a cladding composed of 312 holes of 2.3 μm was employed. Theoretical calculations estimated a yield of 6.5% at a wavelength of 650 nm. The HC-PCF was cut (16 mm) and was integrated in a PMMA microchip. Techniques involving electrostatic coupling were employed to immobilize the DNA in the holes of the MOF. After attaching, signals corresponding to the DNA were detected by comparing with a reference. Although this device possessed acceptable robustness, a temperature control was proposed in order to improve its performance [148]. Sun et al. incorporated a SC-PCF in an electrophoresis microchip. By encapsulating the SC-PCF in a PMMA microchip, a complete substitution of the conventional capillary by the SC-PCF was achieved. With this implementation, an enhancement in the microchip

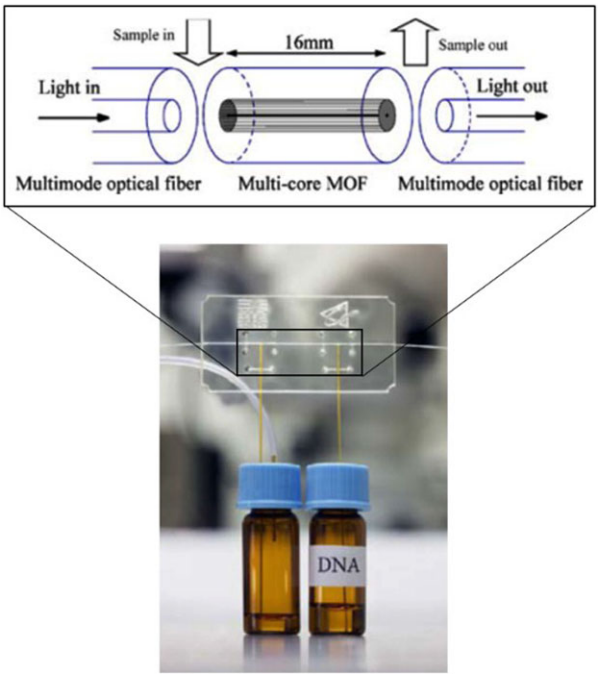

Figure 18 Scheme proposed by the authors where a lab on a chip integrates a MOF, connected to two fibers to guide light. Fluid samples are injected through silica capillary tubes. Above, a scheme of the sensing area of the system is enlarged. Figure taken from [148] with permission of Springer.

performance was achieved since an increase of the separation voltage was possible avoiding at the same time the increase of heat generated (Joule effect). This phenomenon was possible due to the larger cross section of the SC-PCF compared to the conventional capillary, which allowed a better heat dissipation and an improved peak resolution of the substances under study [149]. The authors also employed a microchip with an integrated SC-PCF (ESF-12-01, Blaze Photon. UK) for DNA separation. Taking advantage of the exceptional heat-dissipation properties of PCFs electrical fields up to 1000 V cm^{-1} were sustained, providing better separations. The structure employed had 125 μm OD, and 54 holes of 3.7 μm. A separation length of 7 cm was used in the PMMA microchip. By adding the dye YOPRO-1 in the background electrolyte, fluorescence measurements could be performed to detect DNA fragments. Better resolutions were obtained when using the SC-PCF instead of the conventional capillary for a determined separation voltage [150].

Finally, the implementation of MOFs and microstructures in analytical instrumentation such as HPLC or CE equipment has been carried out. Daley et al. employed SC-PCF as columns for liquid chromatography. Different triphenylphosphine oxides were selected as target analytes. A previous pretreatment of the PCFs was carried out prior their use as chromatographic columns. This treatment consisted of the functionalization of the internal walls of the holes inside the PCFs through covalent attachments to produce a fluorous coating. Figure 19 shows a representative chromatogram where the different compounds were separated and identified. Despite the detection being possible, peak splitting was evidenced due to the different chromatographic behavior of each microchannel [151]. Rogers et al. presented the use of SC-PCFs for CE in a home-made equipment. 4 different SC-PCFs from NKT photonics were employed. The structures had 30, 54, 84 and 168 holes of 4.9, 3.8, 4.3 and 5.6 μm, respectively. The peptides leucine-aveline, leucine-enkephalin and bradykinin were labeled with Cy5 fluorescent dyes. To ensure reproducible electro-osmotic flow, conditioning of the microstructures was performed. The home-made system had a high voltage supply (6 kV) and an excitation laser emitting at 635 nm was employed for fluorescence detection. When focusing on the current generated during the application of the voltage, a decrease of the current values was obtained for all the microstructures when comparing to their respective similar conventional capillaries (similar total cross section). When detecting the different labeled peptides, an increase

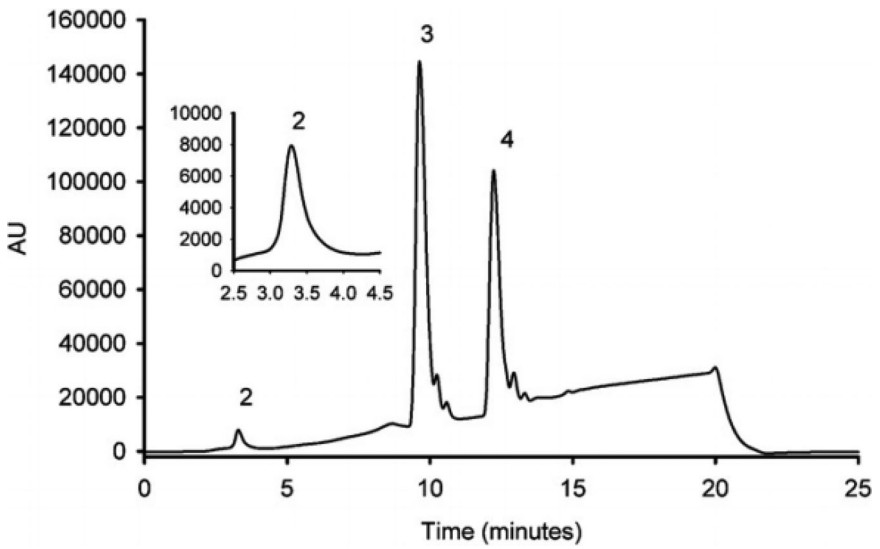

Figure 19 Chromatogram showing three different compounds (2, triphenylphosphine; 3, singly tagged fluorous triphenyelphosphine oxide and 4, double tagged fluorous triphenylphosphine oxide) separated through a 54-hole PCF previously functionalized with monochlorosilane. Figure taken from [151] with permission of Elsevier.

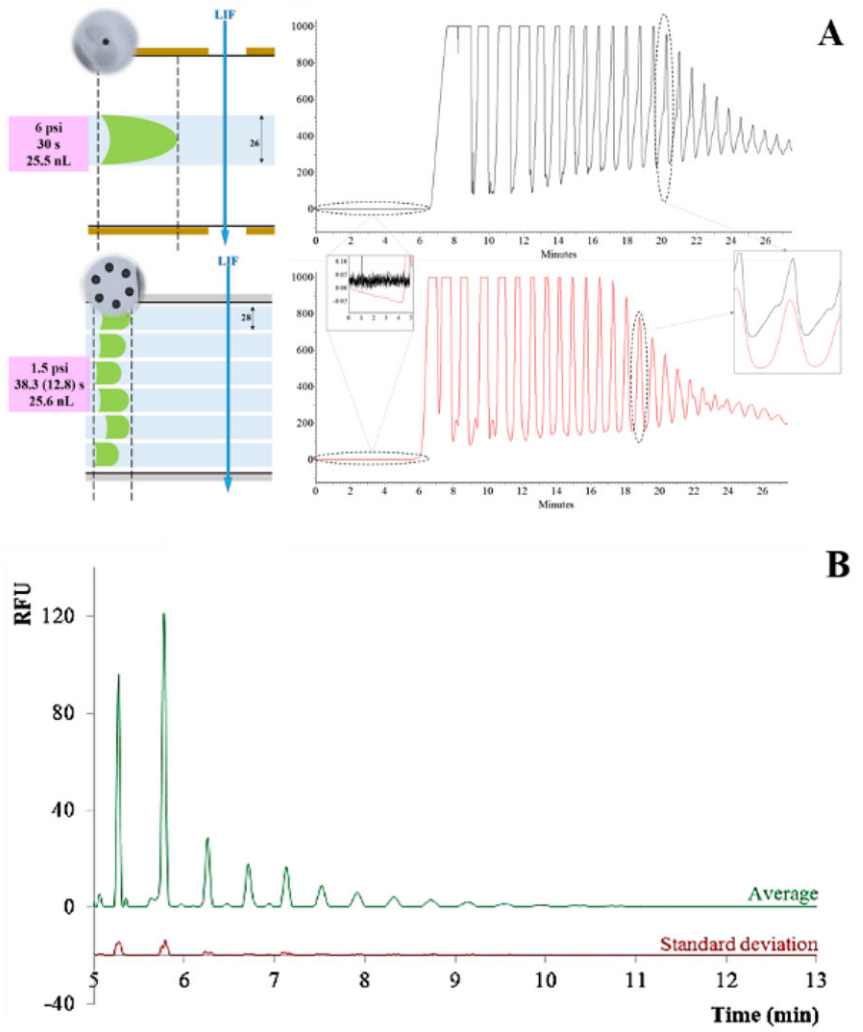

Figure 20 Application of a 6-hole MSC in a commercial CE equipment. (A) comparative of a conventional capillary with a 6-hole MSC for the analysis of starch. Figure taken from [85] with permission of John Wiley & Sons. (B) analysis of dynamite samples where the nitrocellulose profile can be detected by using a 6-hole MSC (red line shows the deviation for an average electropherogram from 10 replicates made during the same day). Figure taken from [153] with permission of Elsevier.

in efficiency (ranging from 20 to 80% of improvement) was evidenced by comparing the 30-hole PCF to the 30-μm ID conventional capillary [152].

Calcerrada et al. employed for the first time a SC-PCF and microstructured capillaries (MS(C) as separation platform in a conventional CE instrument. MSCs are hybrid structures between PCFs and conventional capillaries used in CE, as these structures are manufactured as PCFs (stack-and-draw technique) and possess similar geometry, but they are designed for sensing in fluid media and not to guide light through them. In this study, fluorescein was used as the analyte probe, and different structures were compared (two conventional capillaries, one PCF and one MS(C). Injections were performed by applying a determined pressure. Different analytical parameters were calculated for the three structures, obtaining similar results. When injecting minimal values, improvements in peak asymmetry and linearity were also evidenced for the MSC, overall when comparing this structure with the transparent coated capillary [114]. The same authors also developed a 6-hole MSC with 24.5 μm ID to analyze more complex samples such as derivatized polymeric structures, which provide a characteristic elctropherogram (a group of decreasing peaks along the time). It was proven that the hydrodynamic behavior of the 6-hole capillary was not equal to conventional capillaries, and a correction factor was needed to inject volume samples similar to conventional structures. By injecting similar volume values of starch, the CE performance of the MSC was compared to that from conventional capillaries. Figure 20A shows electropherograms obtained with a 25-μm ID conventional capillary and the 6-hole MSC. More symmetric peaks and a reduction of noise were evidenced when using the MSC. A first application was also demonstrated by successfully detecting the polymeric profile of Nitrostarch [98]. Finally, taking advantage of the properties of the 6-hole MSC, a method optimization was made for the detection of nitrocellulose contained in real dynamite samples, which had never been detected before by CE. With the method developed, amounts in the order of 250–400 pg of nitrocellulose were detected. Figure 20B shows an average electropherogram of one sample of dynamite analyzed under the optimized conditions, as well as the standard deviation relative to the intensity of each peak from the polymeric profile [153].

6. Concluding remarks

This manuscript collects and discusses recent literature on the use of MOFs and related microstructures for chemical and biochemical sensing applications in fluid media. Despite the fact that many types of structures have been employed for this purpose, SC-MOFs and HC-MOFs have proven to be the most studied systems. Nevertheless, other microstructures, such as multihole silica capillaries and other original designs have been proposed to enhance the sensing performance. With regard to the detection systems, fluorescence and Raman spectroscopy have been the techniques selected, as the properties of MOFs can enhance the performance of these optical techniques.

The use of MOFs and microstructures present some advantages in the field of analytical chemistry and sensing. The sample volumes needed are minimal compared to conventional systems such as cuvettes. This is not only interesting from a green-chemistry perspective, but it is also essential when attempting the detection of analytes in minimal sample amounts, usually found in some fields like biological or forensic analysis. In addition, taking advantage of the enhancement of sensitivity with these microstructures, detection of extremely low sample concentrations is possible. This is due to the longitudinal detection of the samples and the low transmission losses along the structures. Moreover, the inner surface of the internal holes of these structures can be chemically activated, thus allowing the detection of biomolecules or the use of SERS for even a higher detection enhancement.

As the implementation of MOFs and related microstructures in conventional analytical instrumentation is a challenge, new studies regarding the use of these structures in lab-on-a-chip technologies as well as in commercial equipment have been proposed. The unique properties that MOFs can provide for sensing enhancement may be of great importance for a future improvement in the performance of current analytical methodologies.

Received: 23 February 2015, **Revised:** 9 September 2015, **Accepted:** 3 May 2015

Published online: 6 November 2015

Key words: Optical fiber, MOF, hollow-core fiber, suspended-core fiber, chemical sensing, sensors, biosensing, microchip.

References

[1] K. C. Kao, T. W. Davies, and R. Worthington, J. I. Electron. Rad. Eng. **39**, 105–111 (1970).
[2] K. C. Kao, J. Electrochem. Soc. **125**, C347 (1978).
[3] M. M. Ramsay, G. A. Hockham, and K. C. Kao, Electron. Commun. **50**, 162–169 (1975).
[4] K. C. Kao and G. A. Hockham, Proc. IEE **7**, 1151–1158 (1966).
[5] P. St. J. Russell, Phys. World **5**, 37–42 (1992).
[6] P. St. J. Russell and J.-L. Archambaul, J. Phys. III **4**, 2471–2491 (1994).
[7] J. D. Joannopoulos, R. D. Meade, and J. N. Winn (eds.) Photonic Crystals: Molding the Flow of Light (Princeton University Press, Princeton, 2008).
[8] J. C. Knight, T. A. Birks, P. St. J. Russell, and D. M. Atkin, Opt. Lett. **21**, 1547–1549 (1996).
[9] P. St. J. Russell, Science **17**, 358–362 (2003).
[10] T. G. Giallorenzi, J. A. Bucaro, A. Dandridge, G. H. Sigel, J. H. Cole, S. C. Rashleigh, and R. G. Priest, IEEE J. Quantum Electron. **18**, 626–665 (1982).
[11] W. R. Setiz, Anal. Chem. **56**, 16A–34A (1984).
[12] W. R. Seitz and M. J. Sepaniak, Crit. Rev. Anal. Chem, **19**, 135–173 (1988).
[13] J. I. Peterson and G. G. Vurek, Science **224**, 123–127 (1984).
[14] T. J. Hall, Electron. Lett. **15**, 405–406 (1979).
[15] P. Polynkin, A Polynkin, N. Peyghambarian, and M. Mansuripur, Opt. Lett. **30**, 1273–1275 (2005).
[16] M. El-Sherif, L. Bansal, and J. Yuan, Sensors **7**, 3100–3118 (2007).
[17] J. Lim, Q. P. Yang , B. E. Jones, and P. R. Jackson, Sens. Actuators A-Phys. **92**, 102–108 (2001).
[18] S. Zheng, Y. Zhu, and S. Krishnaswamy, Sens. Actuators B-Chem. **176**, 264–274 (2013).
[19] K. B. Mogensen and J. P. Kutter, Electrophoresis **30**, S92–S100 (2009).
[20] X. Fan and I. M. White, Nature Photon. **5**, 591–597 (2011).
[21] O. S. Wolfbeis, Anal. Chem. **80**, 4269–4283 (2008).
[22] X. Fan, I. M. White, S. I. Shopova, H. Zhu, J. D. Suter, and Y. Sun, Anal Chim. Acta **620**, 8–26 (2008).
[23] A. M. Cubillas, S. Unterkofler, T. G. Euser, B. J. M. Etzold, A. C. Jones, P. J. Sadler, P. Wasserscheid, and P. St. J. Russell, Chem. Soc. Rev. **42**, 8629–8648 (2013).
[24] G. Emiliyanov, P. E. Høiby, and O. Bang, Sensors **13**, 3242–3251 (2013).
[25] T. M. Monro, D. J. Richardson, and P. J. Bennett, Electron. Lett. **35**, 1188–1189 (1999).
[26] T. M. Monro, W. Belardi, K. Furusawa, J. C. Baggett, N. G. R. Broderick, and D. J. Richardson, Meas. Sci. Technol. **12**, 854–858 (2001).
[27] Y. Zhu, H. Du, and R. Bise, Opt. Exp. **14**, 3541–3546 (2006).
[28] M. K. K. Oo, Y. Han, J. Kanka, S. Sukhishvili, and H. Du, Opt. Lett. **35**, 466–468 (2010).
[29] J. C. Knight, J. Broeng, T. A. Birks, and P. St. J. Russell, Science **282**, 1476–1478 (1998).
[30] R. F. Cregan, B. J. Mangan, J. C. Knight, T. A. Birks, P. St. J. Sussell, P-J. Roberts, and D. C. Allan, Science **285**, 1537–1539 (1999).
[31] F. Benabid, J. C. Knight, G. Antonopoulos, and P. St. J. Russell, Science **298**, 399–402 (2002).
[32] J. M. Fini, Meas. Sci. Technol. **15**, 1150–1128 (2004).
[33] T. Ritari, J. Tuominen, H. Ludvigsen, J. C. Petersen, H. Sorensen, T. P. Hansen, and H. R. Simonsen, Opt. Exp. **12**, 4080–4087 (2004).
[34] F. M. Cox, A. Aryros, M. C. J. Large, and S. Kalluri, Opt. Exp. **15**, 13675–13681 (2007).
[35] P. M. Dower, P. M. Farrell, and B. C. Gibson, Syst. Control Lett. **56**, 634–645 (2007).
[36] R. M. Chyad, M. Z. M. Jafri, and K. Ibrahim, Adv. Mater. Res. **626**, 1027–1032 (2012).

[37] P. S. Kumar, C. P. G. Vallabhan, V. P. N. Nampoori, V. N. S. Pillai, and P. Radhakrishnan, J. Opt. A Pure Appl. Opt. **4**, 247–250 (2002).
[38] M. Barth, H. Bartelt, and O. Benson, Fluid-filled optical fibers, in Handbook of Optofluidics (CRC Press, Boca Raton, 2010), Chap 15.
[39] E. Sinchenko, W. E. K. Gibbs, A. P. Mazzolini, and P. R. Stoddart, J. Light. Technol. **31**, 3251–3257 (2013).
[40] W. Cao and Y. Duan, Sens. Actuators B-Chem. **119**, 363–369 (2006).
[41] R. Bharadwaj and S. Mukherji, Sens. Actuators B-Chem. **192**, 804–811 (2014).
[42] J. Luo, J. Yao, W. Wang, X. Zhuang, W. Ma, and Q. Lin, Symp. Photoelectron. Detect. Imaging 2013 Fiber Opt. Sensors Opt. Coherence Tomogr. (SPIE 2013), p. 891412 (2013).
[43] H. Waechter, J. Litman, A. H. Cheung, J. A. Barnes, and H.-P. Loock, Sensors **10**, 1716–1742 (2010).
[44] C. L. Linslal, P. M. Syam-Mohan, A. Halder, and T. K. Gangopadhyay, Sens. Actuators A-Phys. **194**, 160–168 (2013).
[45] M. Kaya, P. Sahay, and C. Wang, Sens. Actuators B-Chem. **176**, 803–810 (2013).
[46] C. Wang, M. Kaya, and C. Wang, J. Biomed. Opt. **17**, 037004 (2012).
[47] D. K. C. Wu, B. T. Kuhlmey, and B. J. Eggleton, Opt. Lett. **34**, 322–324 (2009).
[48] H. W. Lee, M. A. Schmidt, P. Uebel, H. Tyagi, N. Y. Joly, M. Scharrer, and P. St. J. Russell, Opt. Exp. **19**, 8200–8207 (2011).
[49] Y.-H. Tai and P.-K. Wei, Opt. Lett. **35**, 944–946 (2010).
[50] R. M. Verdaasdonk and C. Borst, C. Optics of fiber and fiber probes. In Optical-Thermal Response of Laser-Irradiated Tissue (Plenum, New York, 1995), pp. 619–666.
[51] Y. Zhu, X. Chen, and A. Wang, Opt. Lett. **34**, 2808–2810 (2009).
[52] Z. L. Ran, Y. J. Rao, W. J. Liu, X. Liao, and K. S. Chiang, Opt. Exp. **16**, 2252–2263 (2008).
[53] Y.-J. Chang, Y.-C. Chen, H.-L. Kuo, and P.-K. Wei, J. Biomed. Opt. **11**, 014032 (2006).
[54] D. J. Lipomi, R. V. Martinez, M. A. Kats, S. H. Kang, P. Kim, J. Aizenberg, F. Capasso, and G. M. Whitesides, Nano Lett. **11**, 632–636 (2011).
[55] X. Zheng, D. Guo, Y. Shao, S. Jia, S. Xu, B. Zhao, W. Xu, C. Corredor, and J. R. Lombardi, Langmuir **24**, 4394–4398 (2008).
[56] G. F. S. Andrade, M. Fan, and A. G. Brolo, Biosens. Bioelectron. **25**, 2270–2275 (2010).
[57] G. F. S. Andrade, J. G. Hayashi, M. M. Rahman, W. J. Salcedo, C. M. B. Cordeiro, and A. G. Brolo, Plasmonics **8**, 1113–1121 (2013).
[58] J. Goicoechea, C. R. Zamarreño, I. R. Matías, and F. J. Arregui, Sens. Actuators B-Chem. **132**, 305–311 (2008).
[59] V. Salazar-Haro, V. Márquez-Cruz, and J. Hernández-Cordero, Proc. SPIE **8011**, 80114W, 80114W-10 (2011).
[60] A. Preter, R. A. Katims, V. Artel, C. N. Sukenik, D. Donlagic, and A. Zadok Opt. Mater. Exp. **4**, 903–915 (2014).
[61] L. C. Chin, B. C. Wilson, W. M. Whelan, and I. A. Vitkin, Opt. Lett. **29**, 959–961 (2004).
[62] D. J. Dickey, R. B. Moore, D. C. Rayner, and J. Tulip, Phys. Med. Biol. **46**, 2359–2370 (2001).
[63] Y. Guo, M. K. K. Oo, K. Reddy, and X. Fan, ACS Nano **6**, 381–388 (2011).
[64] F. Chu, G. Tsiminis, N. A. Spooner, and T. M. Monro, Sens. Actuators B-Chem. **199**, 22–26 (2014).
[65] V. V. R. Sai, T. Kundu, and S. Mukherji, Biosens. Bioelectron. **24**, 2804–2809 (2009).
[66] A. Amezcua-Correa, J. Yang, C. E. Finlayson, A. C. Peacock, J. R. Hayes, P. J. A. Sazio, J. J. Baumberg, and S. M. Howdle, Adv. Func. Mater. **17**, 2024–2030 (2007).
[67] M. K. K. Oo, Y. Han, R. Martini, S. Sukhishvili, and H. Du, Opt. Lett. **34**, 968–970 (2009).
[68] X. Yang, C. Shi, R. Newhouse, J. Z. Zhang, and C. Gu, Int. J. Opt 2011. 1–11 (2011)
[69] H. Yan, C. Gu, G. Yang, J. Liu, G. Jin, J. Zhang, L. Hou, and Y. Yao, Appl. Phys. Lett. **89**, 204101.1–204101:3 (2006).
[70] Y. Zhang, C. Shi, C. Gu, L. Seballos, and J. Z. Zhang, Appl. Phys. Lett. **90**, 193504:1–193504:3 (2007).
[71] C. Shi, C. Lu, C. Gu, L. Tian, R. Newhouse, S. Chen, and J. Z. Zhang, Appl. Phys. Lett. **93**, 153101-1–3 (2008).
[72] X. Yang, C. Gu, F. Qian, Y. Li, and J. Z. Zhang, Anal. Chem. **83**, 5888–5894 (2011).
[73] U. S. Dinish, C. Y. Fu, K. S. Soh, R. Bhuvaneswari, A. Kumar, and M. Olivo, Biosens. Bioelectron. **33**, 293–298 (2012).
[74] Y-J. He, Sens. Actuators B-Chem. **193**, 778–787 (2014).
[75] J. Homola, S. S. Yee, and G. Gauglitz, Sens. Actuators B-Chem. **54**, 3–15 (1999).
[76] C. Y. Tsai, S. P. Lu, J. W. Lin, and P. T. Lee, Appl. Phys. Lett. **98** 153108 (2011).
[77] R. Marty, G. Baffou, A. Arbouet, C. Girard, and R. Quidant, Opt. Exp. **18** 3035–3044 (2010).
[78] H. Y. Lin, C. H. Huang, C. H. Chang, Y. Chiang Lan, and H. C. Chui, Opt. Exp. **18** 165–172 (2010).
[79] S. J. Yoon and D. Kim, J. Opt. Soc. Am. A, **25**, 725–735 (2008).
[80] Y. J. He, Opt. Exp. **21**, 13875–13895 (2013).
[81] P. Bhatia and B. D. Gupta, Appl. Opt. **50**, 2032–2036 (2011).
[82] L. Y. Shao, Y. Shevchenko, and J. Albert, Opt. Exp. **18**, 11464–11471 (2010).
[83] M. Y. Ng and W. C. Liu, Opt. Exp. **17**, 5867–5878 (2009).
[84] Y. S. Jung, J. Wuenschell, H. K. Kim, P. Kaur, and D. H. Waldeck, Opt. Exp. **17**, 16081–16091 (2009).
[85] Y. Lin, Y. Zou, Y. Mo, J. Guo, and R. G. Lindquist, Sensors **10**, 9397–9406 (2010).
[86] B. Sciacca and T. M. Monro, Langmuir **30**, 946–954 (2014).
[87] R. Dutta, R. Bharadwaj, S. Mukherji, and T. Kundu, Appl. Opt. **50**, E138–E144 (2011).
[88] Y. Liu, Y. Zou, and R. G. Lindquist, Biomed. Opt. Exp. **2**, 478–484 (2011).
[89] Y. J. He, Opt. Exp. **21**, 23498–23510 (2013).
[90] A. Wang, A. Docherty, B. T. Kuhlmey, F. M. Cox, and M. C. J. Large, Opt. Lett. **34**, 3890–3892 (2009).
[91] A. L. Huston and J. D. Eversole, Opt. Lett. **18**, 1104–1106 (1993).
[92] S. T. Chu, W. Pan, S. Sato, T. Kaneko, B. Little, and Y. Kokubun, IEEE Photon. Technol. Lett. **11**, 688–690 (1999).
[93] A. Boleininger, T. Lake, S. Hami, and C. Vallance, Sensors **10**, 1765–1781 (2010).

[94] G. Z. Xiao, A. Adnet, Z. Y. Zhang, F. G. Sun, and C. P. Grover, Sens. Actuators A-Phys. **118**, 177–182 (2005).
[95] T. Wey, Y. Han, Y. Li, H-L. Tsay, and H. Xiao, Opt. Exp. **16**, 5764–5769 (2008).
[96] T. Wieduwilt, J. Dellith, F. Talkenberg, H. Bartelt, and M. A. Schmidt, Opt. Exp. **22**, 25333–25346 (2014).
[97] J. C. Knight, T. A. Birks, P. St. J. Russell, and D. M. Atkin, Opt. Lett. **21**, 1547–1549 (1996).
[98] M. Calcerrada, M. A. Fernández de la Ossa, P. Roy, M. González-Herráez, and C. García-Ruiz, Electrophoresis **36**, 433–440 (2015).
[99] M. A. V. Eijkelenborg, M. C. J. Large, A. Argyros, J. Zagari, S. Manos, N. A. Issa, I. Bassett, S. Fleming, R. C. McPhedran, C. M. D. Sterke, and N. A.P. Nicorovici, Opt. Exp. **9**, 319–327 (2001).
[100] M. Becker, M. Werner, O. Fitzau, D. Esser, J. Kobelke, A. Lorenz, A. Schwuchow, M. Rothhardt, K. Schuster, D. Hoffmann, and H. Bartelt, Opt. Fiber Technol. **19**, 482–485 (2013).
[101] L. Xiao, W. Jin, M. Demokan, H. Ho, Y. Hoo, and C. Zhao, Opt. Exp. **13**, 9014–9022 (2005).
[102] F. M. Cox, R. Lwin, M. C. J. Large, and C. M. B. Cordeiro, Opt. Exp. **15**, 11843–11848 (2007).
[103] C. M. B. Cordeiro, M. A. R. Franco, G. Chesini, E. C. S. Barretto, R. Lwin, C. H. B. Cruz, and M. C. J. Large, Opt. Exp. **14**, 13056–13066 (2006).
[104] Y. Ruan, E. P. Schartner, H. Ebendorff-Heidepriem, P. Hoffmann, and T. M. Monro, Opt. Exp. **15**, 17819–17826 (2007).
[105] Y. Lu, C.-J. Hao, B.-Q. Wu, M. Musideke, L.-C. Duan, W.-Q. Wen, and J.-Q. Yao, Sensors **13**, 956–965 (2013).
[106] Y. Ruan, T. C. Foo, S. Warren-Smith, P. Hoffmann, R. C. Moore, H. Ebendorff-Hedepriem, and T. M. Monro, Opt. Exp. **16**, 18514–18526 (2008).
[107] H. K. Tyagi, M. A. Schmidt, S. L. Prill, and P. St. J. Russell, Opt. Exp. **16**, 17227–17236 (2008).
[108] W. Yuan, L. Khan, D. J. Webb, K. Kalli, H. K. Rasmussen, A. Stefani, and O. Bang, Opt. Exp. **19**, 19731–19739 (2011).
[109] K. Nielsen, H. K. Rasmussen, A. J. L. Adam, P. C. M. Planken, O. Bang, and P. U. Jepsen, Opt. Exp. **17**, 8592–8601 (2009).
[110] I. P. Johnson, W. Yuan, A. Stefani, K. Nielsen, H. K. Rasmussen, L. Khan, D. J. Webb, K. Kalli, and O. Bang, Electron. Lett. **47**, 271–272 (2011).
[111] Y. Zhu, R. T. Bise, J. Kanka, P. Peterka, and H. Du, Opt. Commun. **281**, 55–60 (2008).
[112] X. Yu, Y. Sun, G. B. Ren, and P. Shum, IEEE Phot. Technol. Lett. **20**, 336–338 (2008).
[113] D. Pristinski and H. Du, Opt. Lett. **31**, 3246–3248 (2006).
[114] M. Calcerrada, P. Roy, C. Garcia-Ruiz, and M. González-Herráez, Sens. Actuators B-Chem. **191**, 264–269 (2014).
[115] K. Nielsen, D. Noordengraaf, T. Sorensen, A. Bjarklev, and T. P. Hansen, J. Opt. A Pure Appl. Opt, **7**, L13–L20 (2005).
[116] R. Kostecki, H. Ebendorff-Heidepriem, C. Davis, G. McAdam, S. C. Warren-Smith, and T. M. Monro, Opt. Mater. Exp. **2**, 1538–1547 (2012).
[117] F. Wang, W. Yuan, O. Hansen, and O. Bang, Opt. Exp. **19**, 17585–17590 (2011).
[118] S. O. Konorov and A. M. Zheltikov, Opt. Exp. **13**, 3454–3459 (2005).
[119] C. M. B. Cordeiro, E. M. dos Santos, C. H. Brito-Cruz, C. J. S. de Matos, and D. S. Ferreira, Opt. Exp. **14**, 8403–8412 (2006).
[120] A. Khetani, V. S. Tiwari, A. Harb, and H. Anis, Opt. Exp. **19**, 15244–15254 (2011).
[121] G. O. S. Williams, T. G. Euser, P. St. J. Russell, and A. C. Jones, Methods Appl. Fluor. **1**, 015003–015010 (2013).
[122] J. B. Jensen, P. E. Hoiby, G. Emiliyanov, O. Bang, L. H. Pedersen, and A. Bjarklev, Opt. Exp. **13**, 5883–5889 (2005).
[123] Z. Xie, Y. Lu, H. Wei, J. Yan, P. Wang, and H. Ming, Appl. Phys B **95**, 751–755 (2009).
[124] C. Martelli, J. Canning, D. Stocks, and M. J. Crossley, Opt. Lett. **31**, 2100–2102 (2006).
[125] L. Rindorf, J. B. Jensen, M. Dufva, L. Hagsholm-Pedersen, P. Erik-Hoiby, and O. Bang, Opt. Exp. **14**, 8224–8231 (2006).
[126] J.-N. Wang and J.-L. Tang, Sensors **12**, 2983–2995 (2012).
[127] T. M. Monro, S. Warren-Smith, E. P. Schartner, A. François, S. Heng, H. Ebendorff-Heidepriem, and S. Afshar, Opt. Fiber Technol. **16**, 343–356 (2010).
[128] T. G. Euser, J. S. Y. Chen, N. J. Farrer, M. Scharrer, P. J. Sadler, and P. St.J. Russell, J. Appl. Phys. **103**, 103108-1–3 (2008).
[129] G. Emiliyanov, J. B. Jensen, O. Bang, P. E. Hoiby, L. H. Pedersen, E. M. Kjaer, and L. Lindvold, Opt. Lett. **32**, 460–463 (2007).
[130] H. Yan, J. Liu, C. Yang, G. Jin, C. Gu, and L. Hou, Opt. Exp. **16**, 8300–8305 (2008).
[131] J. R. Ott, M. Heuck, C. Agger, P. D. Rasmussen, and O. Bang, Opt. Exp. **16**, 20834–20847 (2008).
[132] M. H. Frosz, A. Stefani, and O. Bang, Opt. Exp. **19**, 10471–10484 (2011).
[133] F. Benabid, J. C. Knight, and P. St. J. Russell, Opt. Exp. **10**, 1195–1203 (2002).
[134] S. Smolka, M. Barth, and O. Benson, Opt. Exp. **15**, 12783–12791 (2007).
[135] V. K. Shinoj and V. M. Murukeshan, Opt. Photon. J. **1**, 85–90 (2011).
[136] V. K. Shinoj and V. M. Marukeshan, J. Appl. Phys. **111**, 023106 (2012).
[137] P. Ghenuche, H. Rigneault, and J. Wenger, Opt. Exp. **20**, 28379–28387 (2012).
[138] X. Yang, A. Y. Zhang, D. A. Wheeler, T. C. Bond, C. Gu, and Y. Li, Anal. Bioanal. Chem. **402**, 687–691 (2012).
[139] J. B. Jensen, L. H. Pedersen, P. E. Hoiby, L. B. Nielsen, T. P. Hansen, J. R. Folkenberg, J. Riishede, D. Noordgraaf, K. Nielsen, A. Carlsen, and A Bjarklev, Opt. Lett. **29**, 1974–1976 (2004).
[140] J. Park, S. Lee, S. Lee, S. E. Kim, and K. Oh, Opt. Exp. **20**, 5281–5290 (2012).
[141] S. H. Kassani, J. Park, Y. Jung, J. Kobelke, and K. Oh, Opt. Exp. **21**, 14074–14083 (2013).
[142] F. Knorr, D. R. Yankelevich, J. Liu, S. Wachsmann-Hogiu, and I. Marcu, J. Biophoton. **5**, 14–19 (2012).
[143] C. Markos, W. Yuan, K. Vlachos, G. E. Town, and O. Bang, Opt. Exp. **19**, 7790–7798 (2011).

[144] G. E. Town, Q. Yuan, R. McCosker, and O. Bang, Opt. Lett. **35**, 856–858 (2010).
[145] W. Yuan, G. E. Town, and O. Bang, IEEE Sens. J. **10**, 1192–1198 (2010).
[146] H. Aouani, F. Deiss, J. Wenger, P. Ferrand, N. Sojic, and H. Rigneault, Opt. Exp. **17**, 19085–19092 (2009).
[147] Y. Guo, H. Li, K. Reddy, H. S. Shelar, V. R. Nittoor, and X. Fan, Appl. Phys. Lett. **98**, 041104-1–3 (2011).
[148] L. Rindorf, P. E. Hoiby, J. B. Jensen, L. H. Pedersen, O. Bang, and O. Geschke, Anal. Bioanal. Chem. **385**. 1370–1375 (2006).
[149] Y. Sun, Y. C. Kwok, and N.-T. Nguyen, Electrophoresis **28**, 4765–4768 (2007).
[150] Y. Sun, N.-T. Nguyen, and Y. C. Kwok, Anal. Bioanal. Chem. **394**, 1707–1710 (2009).
[151] A. B. Daley, R. D. Wright, and R. D. Oleschuk, Anal. Chim. Acta **690**, 253–262 (2011).
[152] B. Rogers, G. T. T. Gibson, and R. D. Oleschuik, Electrophoresis **32**, 223–229 (2011).
[153] M. Calcerrada, M. A. Fernández de la Ossa, P. Roy, M. González-Herráez, and C. García-Ruiz, Microch. J. **123**, 218–223 (2015).